8-19-2021 1:00 PM

Examining the role of Chloride Homeostasis and PGE2 signaling in the Neuroendocrine stress response to inflammation

Samuel A. Mestern, *The University of Western Ontario*

Supervisor: Inoue, Wataru, *The University of Western Ontario*

A thesis submitted in partial fulfillment of the requirements for the Master of Science degree in Neuroscience

Abstract

The brain senses inflammatory signals and drives the release of glucocorticoids (GCs) — potent immunosuppressants— via the activation of the hypothalamic-pituitary-adrenal (HPA) axis. This inflammation induced HPA axis activation is largely mediated by prostaglandin E2 (PGE2), acting on two subtypes of the PGE2 receptor, EP1 and EP3. Recently, our group revealed EP3 signaling mechanisms that excite HPA axis regulatory neurons. This thesis sought to tease out the remaining EP1 signaling mechanisms. Considering that the excitability of HPA axis regulatory neurons is constrained by $GABA_A$ receptor-mediated synaptic inhibition that relies on low-level intracellular Cl^-. We hypothesized that PGE2-EP1 signaling impairs $GABA_A$ receptor-mediated inhibition by increasing intracellular Cl^- levels. We used two electrophysiological approaches (perforated patch and whole-cell recordings) and showed that PGE2 depolarizes the reversal potential of $GABA_A$ receptor currents (E_{GABA}), an indicator of intracellular Cl^- elevation. The effect of PGE2 was mimicked by EP1 agonist and prevented by EP1 antagonist. The depolarizing shift was slow to develop but became significant by 20 min post PGE2. Our results indicate that PGE2-EP1 coupling induces a slow depolarizing shift in E_{GABA} for the excitation of PVN-CRH neurons during inflammation.

Keywords

Stress, Neuroendocrinology, Neuroimmune, GABA, hypothalamic-pituitary-adrenal axis, HPA, paraventricular nucleus, corticotropin-releasing hormone neurons, prostaglandin E2, inflammation

Lay Summary

When the body encounters an injury or illness, it often goes through an immune process called inflammation. This involves the recruitment of other immune cells to the site of the illness/injury to initiate defence, cleanup, and repair. The body can regulate the inflammation process via the activation of a pathway called the hypothalamic-pituitary-adrenal axis (HPA) axis, which releases hormones called glucocorticoids (GCs) – which are potent immune regulators. The immune system activates the HPA axis by activating a subset of neurons (parvocellular corticotrophin-releasing hormone neurons; PVN-CRH neurons) in a brain region called the hypothalamus. This is achieved via an immune-signalling molecule called prostaglandin (PG)E2. PGE2 is known to act through two distinct (receptor-based) signaling pathways; EP1 & EP3. Previously our group showed how the EP3 pathway disinhibits these neurons, allowing their activation, and driving the HPA axis. This work aims to understand how the EP1 pathway modulates these neurons. We hypothesized that the EP1 pathway shifts the magnitude and direction of inhibition in the PVN-CRH neurons. Using electronic recordings (patch-clamp electrophysiology) from individual neurons, we looked at changes in induced incoming inhibitory signals in these neurons. We found that inhibition magnitude is weakened or even reversed in these neurons in the presence of both PGE2 and iloprost (a chemical mimicking PGE2 that activates the EP1 pathway). Moreover, blocking the EP1 pathway while applying PGE2 partially prevented this effect. We theorized that this weakening of inhibition would lead to disinhibition of the PVN-CRH neurons and activation of the HPA axis. We posited that this EP1 pathway works in compliment to the EP3 pathway to activate the HPA axis during periods of inflammation. In summary, we demonstrated the consequences of PGE2-EP1 signaling in PVN-CRH. In the broader scope, this contributes to our understanding of how inflammation and the brain interface.

Co-Authorship Statement

The experimental works presented in this thesis were conducted by Samuel Mestern under the supervision of Dr. Wataru Inoue.

Acknowledgements

I want to acknowledge and thank my thesis supervisor, Dr. Wataru Inoue, for his guidance during my masters. His patience, helpfulness, and edifying ability cannot be overstated, and his advice has helped guide me throughout graduate school, and towards being a good scientist and scholar. Dr. Inoue was always happy to entertain my ‘out-there’ questions about patch-clamp electrophysiology and enthuse about some cool-but-unexpected results I acquired during my experiments. I also want to thank my former graduate chair Dr. Vania Prado, as well as my committee members Dr. Arthur Brown (and current graduate chair) and Dr. Wei-Yang Lu, for their guiding hand. I want to thank my fellow members of the Inoue Lab, Irma Meleluch, Dr. Hiroyuki Igarashi, Dr. Ahmed Hashad, Aoi Ichiyama, Julia Sunstrum, and Jason Ding. In particular, I want to thank Julia for her help, counsel, and teaching in the ‘rugged’ technique that is patch-clamp electrophysiology; Aoi for always lending an ear and bringing joy & excitement into the lab; and Jason for always being someone I can joke with, or vent to.

Dedication

To Ace, Molly, Patch, Tagger, Kirby, and My Parents.

Table of Contents

List of Abbreviations

Abbreviation	Meaning
(m/e)IPSC	(Miniature/Evoked) Inhibitory Postsynaptic Current
V_m	Membrane Potential
Abs	Absolute
ACSF	Artificial Cerebral Spinal Fluid
ACTH	Adrenocorticotropic hormone
AM	Amygdala
AMPA	α-amino-3-hydroxy-5-methyl-4-isoxazolepropionic acid
ANCOVA	Analysis of Covariance
ANOVA	Analysis of Variance
ANS	Autonomic Nervous System
cAMP	Cyclic Adenosine 3',5'-Monophosphate
CAT	Catalogue
Cl^-	Chloride (ion)
CNS	Central Nervous System
COX-(1/2)	Cyclooxygenases
CRFR1	Corticotropin Releasing Hormone Receptor 1
CRH	Corticotropin Releasing Hormone
DF	Degrees of Freedom
DMSO	Dimethylsulfoxide
DNQX	6,7-Dinitroquinoxaline-2,3-dione
E	Epinephrine
E_{GABA}	Equilibrium Potential of $GABA_A$
EP(1-4)	Prostaglandin E2 Receptor (1-4)
EtOH	Ethanol
FIG	Figure
GABA	γ-aminobutyric acid

GC	Glucocorticoid
GR	Glucocorticoid Receptor
GRF	Growth Hormone-releasing Hormone
GW-848687x	6-[2-[5-chloro-2-[(2,4-digluorophenyl)methoxy]phenyl]-1-cyclopenten-1-yl]-2-pyridinecarboxylic acid
HC	Hippocampus
HPA	hypothalamic-pituitary-adrenal *(axis)*
IL-1β	Interleuken-1β
IPSP	Inhibitory Postsynaptic Potential
KCC2	K^+ Cl^- transporter
KO	Knock Out
LPS	Lipopolysaccharide
mM	Millimolar
mRNA	Messenger Ribonucleic Acid
NE	Norepinephrine / Noradrenergic
NKCC1	Na^+ K^+ $2Cl^-$ transporter 1
PFC	Prefrontal Cortex
PGE_2	Prostaglandin E2
PGH	Prostaglandin H_2
PKC	Protein Kinase C
PVN	Paraventricular nucleus
RT-PCR	Realtime Polymerase Chain Reaction
SRIF	Somatostatin
TNFα	Tumor Necrosis Factor α
TRH	Thyrotropin-releasing Hormone
VEH	Vehicle
α1-AR	α1 Adrenergic Receptor
μM	Micromolar
HCO_3^-	Bicarbonate (ion)

List of Tables

List of Figures

Chapter 1

Introduction

The stress response

All living organisms experience a stress response [1]. That is, in response to a hazardous extrinsic or intrinsic challenge, the organism must mount a suitable response to promote its survival. The mammalian stress response – the focus of this thesis – is characterized by two functionally distinct phases [1–3]. First, an immediate response prepares the body for a rapid answer to the stressor – activating in a matter of seconds to minutes [3,4]. This first phase – termed the flight or fight response – is driven primarily by the autonomic nervous system (ANS) [2,3]. The ANS drives defensive changes like increased heart rate, slowed digestion, and dilated pupils [3]. Second, a slower hormonal-based response kicks in after tens of minutes [3]. This response propels several behavioural and physiological consequences to further prepare the body for the stressor [3]. This slower response is driven by the hypothalamic-pituitary-adrenal axis (HPA), a neuroendocrine hormonal cascade culminating in the release of glucocorticoids (GCs) from the adrenal cortex [3].

It should be noted that the stress response is variable among individuals and not as uniform as outlined above. The exact timing and nature of the response can depend on many factors, including stress magnitude, genetic predisposition, and metabolic state [1].

An overview of the HPA axis

The HPA axis, which drives the slower stress response, can be described as follows; This pathway begins from the hypothalamus, more specifically, a nucleus called the paraventricular nucleus of the hypothalamus (PVN). The PVN contains various neuron types with distinct physiological functions [5]. The HPA axis is driven by a specific subpopulation of neurons that express corticotrophin-releasing hormone (CRH) and send their axons to the median eminence [6–8]. CRH is released at the external zone of the median eminence, an exchange point of the hypothalamic releasing factors (including CRH and several others) and the hypophyseal portal circulation [6–8]. CRH gains access through the fenestrated capillary endothelial to the hypophyseal portal circulation that connects the median eminence and the anterior pituitary [6–

8]. In the anterior pituitary, CRH signals to corticotrophs, leading to the release of adrenocorticotropic hormone (ACTH) into the bloodstream [9,10]. Finally, at the endpoint of the axis, ACTH in the blood signals to the adrenal cortex to release glucocorticoids (GCs) [9]. In turn, GCs have several effects on the body [11]. The complete effects of GC on the body are too numerous to cover in this thesis; a non-exhaustive list includes immunomodulation, glucose metabolism modulation, reproductive modulation, and cognitive effects [11,12]. Crucially, GCs also provide negative feedback onto the parvocellular-CRH neurons, the pituitary, and brain areas upstream of parvocellular-CRH neurons, allowing the HPA axis to self-regulate activation [13]. In order to better detail the initiation of the stress response, we will explore the PVN and PVN-CRH neurons in closer detail below.

The anatomy and functions of the PVN

The primary function of the PVN - much like the rest of the hypothalamus - is to provide homeostatic control for the body's various processes [14]. For example, the PVN is known to play a role in metabolic, osmotic, and cardiac regulation - as well as its aforementioned role in the activation of the HPA axis [15]. Reflecting the multiple physiological roles, the PVN contains various neuron types. Classically, PVN neurons are divided into three major classes, based on their axonal projection targets; Parvocellular, Magnocellular, and Preautonomic neurons [13]. These classes are further subdivided into different neuron types based on their neuropeptide/neurotransmitter expression profiles. We will discuss them briefly here:

Parvocellular: As mentioned above, the HPA axis begins with the parvocellular subclass of neurons. They can be distinguished from other (magnocellular) neuroendocrine neurons in the PVN based on their relatively small soma size and projection target [6,16]. These parvocellular neurons project to the median eminence, where they release their functional peptides [6,9]. A subset of parvocellular neurons synthesizes and releases CRH into the median eminence [6,9]. A small subgroup of parvocellular-CRH neurons also co-express vasopressin. However, these neurons are considered parvocellular neurons based on their axonal projection to the median eminence and are distinct from vasopressin-expressing magnocellular neurons [17]. In addition to CRH and vasopressin, parvocellular neurons have also been shown to express other peptides such as thyrotropin-releasing hormone (TRH), somatostatin (SRIF), and growth hormone-releasing hormone (GRF) [9,18].

Magnocellular: Magnocellular neurons are hormone-releasing (neuroendocrine) cells that send projections directly to the posterior pituitary (in contrast to the median eminence-projecting parvocellular neurons), where they release oxytocin and vasopressin [19]. These neurons are distinguished by their larger cell body size relative to other PVN cells [6]. Magnocellular neurons are critical for fluid osmolarity regulation and the milk ejection reflex, the roles being divided up to vasopressin releasing cells and oxytocin releasing cells, respectively [19–23]. In correspondence with this, the magnocellular neurons possess osmo-sensitive ion channels [21,24].

Preautonomic: Preautonomic neurons are non-neuroendocrine. In other words, they project to the brain stem and the spinal cord (instead of blood) and regulate the ANS, hence the 'preautonomic' designation [25]. Pre-autonomic neurons release a range of peptides, including vasopressin, oxytocin, angiotensin II, and CRH [7,15]. Functionally, the preautonomic neurons have been shown to influence cardiac function, blood pressure, and fluid metabolism [22].

The parvocellular neuroendocrine neurons as the gateway of the stress response

The CRH-releasing parvocellular PVN neurons (PVN-CRH neurons) represent the primary initiation point of the HPA axis and, thereby, the primary integrative point of stress in the brain. Historically, PVN-CRH neurons have been well characterized for their role in the stress response. Initially, it was demonstrated that whole ablation of the paraventricular nucleus impaired hormonal response to stress in the subject [8]. Later, with the advent of more specialized techniques, the knockdown of CRH suppressed hormonal response to acute stress [26]. Moreover, the specific knockdown of CRH in the PVN impaired behavioural response to social stressors [27]. The most well-studied function of PVN-CRH neurons is activating the HPA axis via their projection to the median eminence. In addition to this, emerging evidence points towards the importance of CRH release within the PVN via axonal collaterals or somatodendritic release [28]. The physiological roles of intra-PVN CRH release remain unknown.

As the integrative center of the HPA axis, among other endocrine systems, the PVN-CRH neurons receive direct and indirect inputs from across the brain. This includes the cortex, brainstem, limbic system, and adjacent hypothalamic nuclei [3,9,29]. Direct innervations from the brainstem onto PVN-CRH neurons signal physiological homeostatic stressors rather than psychogenic stressors [3]. For example, ascending adrenergic and noradrenergic input from the

nucleus of the solitary tract encodes for physiological stressors like hypoglycemia [3]. In experimental studies, lesions of the norepinephrine (NE) and epinephrine (E) hindbrain neurons that project to the HPA axis resulted in impaired GC response to metabolic but not psychological stressors [30].

'Higher order' anatomical projections convey psychogenic stressors linked to their function. The medial prefrontal cortex (mPFC), hippocampus (HC), and amygdala (AM) are best studied for their role in the cognitive and emotional control of neuroendocrine stress response [31]. The complexity of their innervation to the PVN reflects the complexity of psychogenic stressors. All three regions do not send direct projection to the PVN but send poly-synaptic signals through lower-order GABAergic relays [31]. In general, the hippocampal and mPFC connections provide excitatory input onto GABAergic relays, thereby inhibiting the PVN [31,32]. Experimental lesions of the ventral subiculum of the hippocampus impaired the post-stress recovery of HPA axis activation in rats [33]. Interestingly, the effects of the hippocampal lesions are stressor-specific, with lesions impairing response to psychogenic stressors like restraint stress [32], or novelty [34], but not to systemic stressors like hypoxia [32]. In other words, the hippocampus exerts inhibitory control over the HPA axis primarily when it is activated by psychological stress. The amygdala connections provide inhibitory input onto GABAergic relays; thereby, amygdala activation inhibits the inhibitory interneurons and disinhibits the PVN [32]. The amygdala represents the primary fear center of the brain. In line with this, lesions to the central nucleus of the amygdala impaired HPA axis response to conditioned and contextual fear stimuli (foot shock) [35]. In total, the "indirect" pathway from the higher brain areas to the PVN reflects the complexity of signal integration underlying psychological stressors. Regardless, GABAergic signaling is crucial to PVN function.

GABA is a regulator of the stress response

Anatomically, the majority of inputs to the PVN are GABAergic [16,36]. Upstream brain regions relay their signals through GABAergic interneurons [31,32]. Furthermore, immunoelectron microscopy studies of the PVN reported that 46-62% of all synaptic input to parvocellular neurons were GABAergic [36,37]. Functionally, GABAergic manipulations directly in the PVN resulted in altered HPA axis activation [38,39]. More specifically, $GABA_A$ receptor agonist application attenuated the HPA axis response to restraint stress [39].

Conversely, a blockade of GABAergic signaling alone (via GABA antagonist bicuculline), before stressor application, potentiated HPA axis response to restraint stress [39]. In contrast, glutamate application alone did not evoke a change in HPA axis activation [38]. Instead, glutamate activated (measured via cFos) adjacent GABAergic interneurons [38], demonstrating that GABA acts to constrain glutamate-induced activation of PVN neurons [38]. Noradrenaline mediates its effects – in part – via the GABAergic interneurons, where it has been demonstrated to have a bidirectional effect on GABAergic signaling [40]. These results indicate that, under basal conditions, GABAergic signaling is constraining HPA axis response. In total, both anatomical and functional evidence points towards GABAergic signaling being a potent, tonically active controller of the stress response that provides gating inhibition to the incoming excitatory input [38,39]. Therefore, removal of GABAergic inhibition results in rapid activation of the HPA axis [41]. In other words, GABAergic signaling allows the PVN-CRH neurons to be primed to respond to stress at a moment's notice. In addition, GABA signaling provides brakes onto the HPA axis to resolve activation following acute stress [42]. In part, GC signaling in the brain activates excitatory neurons upstream of the GABAergic interneurons, triggering GABAergic signaling [43]. This, coupled with GC actions on glutamate in the PVN, allows rapid resolution of the stress response [42].

Emerging evidence also points towards local-rapid GABAergic signaling in the PVN that allows rapid PVN-CRH neuron feedback. Experimental studies have demonstrated a local PVN circuit between PVN-CRH neurons and CRFR1 expressing GABA interneurons immediate to the PVN [44]. Knockout of CRFR1 expressing neurons in the PVN attenuated resolution of HPA axis activation [45].

In addition to increasing or decreasing the firing activities of GABAergic neurons upstream of PVN-CRH neurons, stress changes the modulation of the efficacy of GABAergic synaptic transmission (i.e., GABA plasticity) in the PVN. More specifically, stress can increase or decrease the efficacy of GABAergic synaptic transmission via both pre- and postsynaptic mechanisms. For example, acute stress exposure facilitated the induction of GABA synapses potentiation in the PVN via an increase in GABA synapse number, dependent on adrenergic signaling [46]. In contrast, glucocorticoid signaling following acute stress triggered depression of GABAergic signaling via presynaptic mechanisms that depress the release of GABA-containing

synaptic vesicles [42,43]. Following chronic stress, depression of GABAergic signaling is observed [37,47]. One study utilizing patch-clamp electrophysiology found a decrease in miniature inhibitory postsynaptic current (mIPSC) frequency and amplitude, attributed to a reduction in GABA synapses [48]. Another study found an overall increase in GABAergic and glutamatergic synapses following chronic stress in rats [36]. More specifically, they observed an overall increase in axodendritic GABAergic synapses but a decrease in axosomatic GABAergic synapses in PVN-CRH neurons [37]. Thus, allowing more temporal and spatial summation of incoming input in the dendrites before reaching the soma. Since patch-clamp recordings of miniature inhibitory postsynaptic currents (mIPSC)'s are taken from the soma, the depression in mIPSC amplitude can be attributed to the loss of axosomatic GABAergic synapses [37]

One well-characterized mechanism of plasticity in GABAergic transmission involves the alterations in chloride homeostasis. The $GABA_A$ receptor, an abundant signaling target of GABA in the brain, is an ion channel permeable primarily to chloride (Cl^-) and bicarbonate (HCO_3^-) ions [49]. In healthy adult brains, as GABA binds to the $GABA_A$ receptor, the channel opens, and chloride ion (Cl^-) flows into the neuron. The influx of negatively charged ions (i.e., Cl^-) causes hyperpolarization of the neuronal membrane. However, this flow is dependent on the electrochemical gradient of Cl^- across the cell membrane. More specifically, the electrochemical gradient is determined by two factors (1) the concentration of Cl^- on either side of the membrane, (2) the membrane potential of the neuron (see methods; Determination of $[Cl^-]_i$). The membrane potential at which there is no net flow through the $GABA_A$ receptor is referred to as the equilibrium potential (E_{GABA}; and represents a correlate of Cl^- gradient (as well as HCO_3^- see methods, and [41,50]]). When the $GABA_A$ receptor opens, Cl^- flows down its electrochemical gradient, attempting to equalize the electrochemical gradient and driving the membrane potential towards E_{GABA}. Changes in the Cl^- concentration gradient can shift E_{GABA}, thus modulating $GABA_A$ – mediated inhibition [41,50].

Chloride homeostasis refers to the neurons' maintenance of this Cl^- concentration gradient. Under basal conditions, the neuron maintains low intracellular Cl^- ($[Cl^-]_i$) levels such that E_{GABA} sits at or below resting membrane potential, driving an influx of Cl^- after $GABA_A$ receptor opening [41]. In comparison, the buildup of intracellular Cl^- can lead to a depolarizing shift in E_{GABA} and extrusion of Cl^- following $GABA_A$ receptor opening and subsequent

depolarization of the neuronal membrane [41]. Such a phenomenon can be seen in the developing forebrain: many neurons lack the functional proteins to maintain Cl^- homeostasis, leading to the buildup of Cl^- within the neuron [51,52]. This causes a depolarizing shift in the E_{GABA}. In turn, the opening of the $GABA_A$ channel allows efflux of Cl^- and causes excitation of the neuron [51,52].

Homeostasis of the Cl^- gradient in the forebrain is driven primarily by two ion cotransporters, NKCC1 (Na^+ K^+ $2Cl^-$ transporter) and KCC2 (K^+ Cl^- transporter) [51]. Each transporter drives Cl^- differently, with NKCC1 importing Cl^- into the neuron (alongside sodium and potassium) and KCC2 exporting Cl^- (while also exporting K^+)[51]. Alterations in NKCC1 and KCC2 function provide a potent mechanism for GABA signaling regulation [53]. As noted earlier, experimental studies have shown that a lack of functional KCC2 early in development prevents the cell from exporting Cl^-, leading to a buildup of intracellular Cl^- and, subsequently, excitatory GABAergic signaling [51]. In other cases, impairment of KCC2 function (and subsequent GABAergic signaling dysfunction) has been linked to disorders such as schizophrenia and epilepsy [54,55].

Notably, changes in E_{GABA} are not limited to early development or pathological conditions. NKCC1 and KCC2 regulation may represent a potent mechanism of GABAergic plasticity. For example, cultured hippocampal neurons demonstrate the ability to depress GABAergic signaling via downregulation of KCC2 function following normal synaptic stimulation [56–58]. Similar activity-induced KCC2 plasticity has been shown in other CNS regions, such as the spinal cord [59] and the ventral tegmental area following stress and immune signaling [60,61].

Critically, plasticity via Cl^- homeostasis has also been demonstrated across the hypothalamus. For example, preautonomic PVN neurons show activity-induced NKCC1 and KCC2 regulation [62]. Similarly, magnocellular PVN neurons show regulation of Cl^- homeostasis before lactation or in response to changes in osmotic homeostasis [63,64]. Importantly, evidence indicates that parvocellular PVN-CRH neurons undergo potent plasticity of Cl^- homeostasis via both NKCC1 and KCC2 modulation [41,47,65–67]. PVN-CRH neurons experience a depolarizing shift in E_{GABA} following acute stress, likely due to a functional impairment of KCC2 via a G_q mediated pathway [65–67]. Further experiments demonstrated that

this change depresses GABA signaling during periods of high synaptic activity due to the accumulation of Cl^- within the neuron [68]. Therefore, GABA signaling is conditionally & temporarily excitatory, facilitating the excitation of the HPA axis following stress. Moreover, following chronic unpredictable mild stress, PVN-CRH neurons show a biphasic shift in Cl^- homeostatic regulation. Initially, the neurons show a temporary decrease in KCC2 protein expression triggering a depolarizing shift in E_{GABA} [47]. Subsequently, the neurons show a return of KCC2 protein expression to basal levels and an increase in NKCC1 expression, facilitating a long-term shift in E_{GABA} [47]. However, it is worth noting that simply quantifying the expression of KCC2 is not enough to infer its function, as KCC2 function is tightly regulated by phosphorylation, meaning KCC2 expression at basal levels may still not be extruding Cl^- as expected [66,68,69]. In sum, the evidence indicates that Cl^- homeostasis is a potent mechanism of GABAergic signaling plasticity for PVN-CRH neurons. Specifically, PVN-CRH neurons appear to use modulation of E_{GABA} in a non-pathogenic way to modulate response to incoming stimuli [41].

The HPA axis, GCs, and the immune system

Inflammation represents one prototypical physiological stress resulting in potent HPA axis activation (Fig. 1 A). Inflammation can be generally described as the body's response to injury or invading pathogens [70]. More specifically, inflammation is the recruitment of immune cells and signaling molecules to the damaged tissue to resolve the infection or injury, and begin the cleanup and repair of the tissue [71]. In response to, say – a bacterial infection – certain immune cells will release cytokines to raise the alarm for the rest of the body [71]. When the magnitude is sufficiently large, activation of inflammatory response in the peripheral tissues, or any parts of the CNS, can send signals to the brain and activate the HPA axis (Fig. 1 A). For example, experimental induction of the inflammation response via lipopolysaccharide (LPS) – a component of the outer membrane of gram-negative bacteria that stimulates an immune response [72–74] – induced potent activation of the HPA axis via the upregulation of inflammatory cytokines (e.g. IL-1β and TNFα) by peripheral immune cells [75]. Direct administration of cytokines (IL-1 β, TNFα) also triggered activation of the HPA axis [76]. Moreover, administration of LPS increased activation of PVN neurons (measured via cFos) and increased circulating levels of corticosterone [77]. Ablation of the PVN impaired ACTH response to LPS

[78]. Thus, inflammation is a powerful physiological stressor inducing the activation of neurons in the PVN.

In turn, the HPA axis facilitates the resolution of the inflammatory response (Fig. 1 A). In other words, the HPA axis provides critical negative feedback onto the immune system during periods of a potent immune response. Overactivation or extended activation of the immune system can be maladaptive, and as such, it is key that the body can regulate this response via negative feedback mechanisms [79]. Consequently, disruption of this ability is thought to be pathogenic in many disorders [79]. In experimental studies, adrenalectomy or hypophyseal lesions impaired HPA axis response to inflammation and increased the lethality [80–82]. This HPA axis regulation is partly mediated by GCs, the hormonal output of the HPA axis, because supplementation of GCs significantly reversed the lethality caused by the surgical disruption of the HPA axis [82]. GCs are potent immunomodulators, exerting numerous effects on the immune system [12,83]. During periods of inflammation, GCs act to repress the synthesis and release of inflammatory cytokines [83]. This is achieved via GC – glucocorticoid receptor (GR) signaling leading to several transcriptional changes [12,83]. Pharmacological blockade of the GR receptor results in adrenalectomized-like lethality due to induced inflammation [84]. However, it should be noted that the roles of GCs in the immune system are very complex [12,83], and extensive discussion on this matter is beyond the scope of this thesis.

Immune-to-PVN signaling via Prostaglandin E2

While the importance of the HPA axis activation during inflammation is extensively documented, exactly how signals from the immune system activate PVN-CRH neurons, and subsequently the HPA axis, remains incompletely understood. Generally, the molecular mechanism appears to involve a two-stage process:

First, inflammatory cytokine signals, reaching the brain through the general circulation, binds to endothelial cells & perivascular macrophages and induce upregulation of the cyclooxygenases pathways (COX-1 and COX-2) [85–87] (Fig. 1 B). Functionally, this means that inflammatory cytokines do not cross the blood-brain barrier themselves, but instead, endothelial cells act as a signal transmission method. Next, activation of COX-1 and COX-2 triggers the synthesis of PGs. More specifically, the COX's are involved with the synthesis of prostaglandin H_2 (PGH), a precursor for various PG subtypes H, I, D, E, F [88–90]. In the HPA

axis activation case, PGH is synthesized into PGE2 [86] (Fig. 1 B). Experimental evidence indicates that PGE2 but not other PGs mediate inflammation-induced activation since the pharmacological blockade or genetic ablation of the PGE2 receptors almost completely prevents HPA activation in response to LPS [86,91]. In turn, PGE2 is then released into the PVN [86,91] (Fig. 1 B). Finally, PGE2 signaling in the PVN induces activation of parvocellular PVN-CRH neurons, and subsequently, the HPA axis [85,86,92] (Fig. 1 B).

PGE2 signals through its four receptor subtypes EP1, EP2, EP3, and EP4 [90]. Across the brain, these receptors mediate differential effects and consequently have distinct downstream signaling mechanisms [89,93]. All four receptors a G-protein coupled receptors. EP2 and EP4 signal through G_s, causing upregulation of cyclic adenosine 3',5'-monophosphate (cAMP)-mediated pathway [89,90,94]. In contrast, the EP3 signaling pathway is a G_i-mediated cAMP down regulator [89]. Finally, EP1 triggers a G_q-mediated intracellular calcium increase and activates the protein kinase C (PKC pathway) [89]. Regarding the activation of the HPA axis, PGE2 primarily exerts its effects through the EP1 and EP3 signaling pathways [91]. In experiments completed in knockout mouse lines for each of the four receptor subtypes, only EP1 and EP3 knockouts showed impaired ACTH response to LPS, whereas EP2 and EP4 knockouts showed responses similar to controls [91] (Fig. 1 B). Further studies revealed that pharmacological antagonism of EP3 impairs the results of PGE2 based activation of PVN-CRH neurons [95,96] (Fig. 1 B). Furthermore, immunohistochemistry, RT-PCR, and *in situ* studies have confirmed EP1 and EP3 receptor subtypes in the PVN [91,95,97,98]. Crucially, such studies have differently localized the two receptors. EP3 has been localized presynaptically in the PVN [91,95,99]. On the other hand, EP1 is localized postsynaptically [91,98]. Some studies also report EP2 and EP4 mRNA localization in the postsynaptic PVN neurons [98,100].

Importantly, the mechanism by which PGE2 modulates PVN activity seems to be GABAergic in nature. Recent work from our lab revealed an EP3-mediated activation of PVN-CRH neurons via GABAergic modulation [99]. Application of PGE2 to *ex vivo* slices attenuated incoming GABAergic signal amplitude [99]. This effect could be diminished via the application of an EP3 antagonist or mimicked via the application of an EP3 agonist [99]. This is congruent with previous work that showed a decrease in miniature IPSC amplitude and inhibitory postsynaptic potential (IPSP) frequency following PGE2 application [86] (Fig. 1 B). Subsequent

to this, there was a depolarization of the membrane potential of PVN-CRH neurons and an increase in firing frequency [86]. Such results indicate that PGE2, much like other stressors, activates the HPA axis by inhibiting incoming GABAergic connections, thereby disinhibiting the PVN-CRH neurons. Thus, our work and those by others (Ferri and Ferguson, 2005; Zhang et al., 2011) established that the PGE2-EP3 signaling mechanism involves inhibiting GABA release from the presynaptic terminals to the postsynaptic PVN-CRH neurons, thereby reducing the amount of inhibition (i.e., disinhibition) (Fig. 1 B). However, a previous EP receptor subtype-specific KO study also indicated an indispensable role of EP1 [91]. The molecular and cellular mechanistic role of EP1 in mediating activation of the HPA axis is unclear. To better understand how the HPA axis and the immune system are coupled, it is critical to understand the role of EP1 signaling in the PVN.

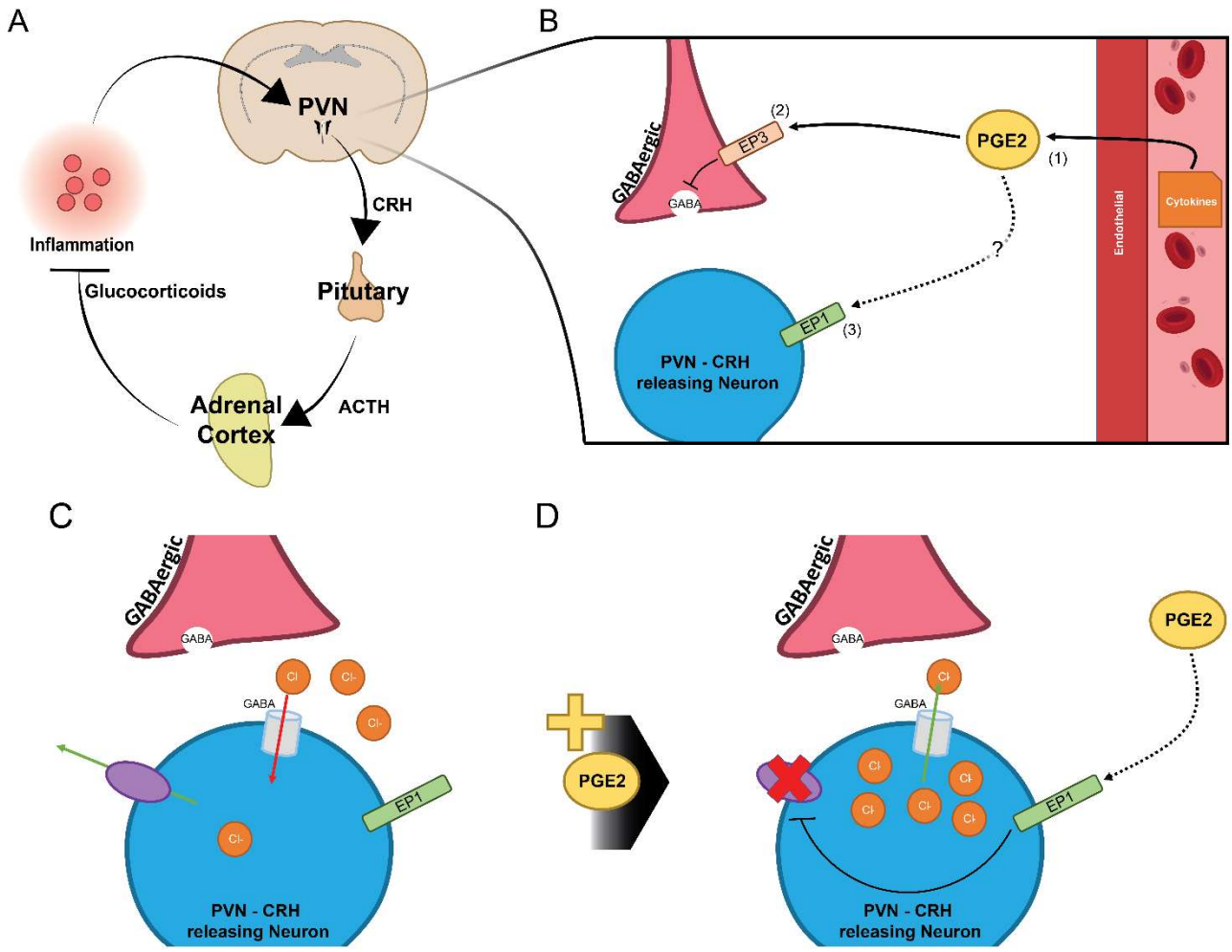

FIG 1 - Hypothesis: PGE2 changes $GABA_A$ receptor reversal potential via EP1 signaling in PVN-CRH neurons

(A) Schematic representation of the inflammation to hypothalamic-pituitary-adrenal (HPA) axis communication. In short, inflammation induces the release of corticotrophin-releasing hormone (CRH) from the paraventricular nucleus (PVN) of the hypothalamus. This triggers the release of adrenocorticotropic hormone (ACTH) from the pituitary. In turn, ACTH stimulates the release of glucocorticoids (GCs) from the adrenal cortex. GCs provide regulatory feedback to the inflammatory response. (B) Schematic representation of the inflammation-mediated activation of the PVN-CRH neurons. (1) Circulating cytokines trigger the release of prostaglandin E2 (PGE2; yellow) into the PVN [86]. (2) PGE2 acting via its EP3 receptor (orange) presynaptically inhibits GABAergic (red) signaling, disinhibiting PVN-CRH neurons (blue) [86,91,99]. (3) Knockout

studies showed the EP1 (expressed postsynaptically in PVN-CRH neurons; green) is necessary for mediating the HPA axis response to inflammation [91,98]. (C & D) Schematic representation of our hypothesis: PGE2 changes $GABA_A$ receptor reversal potential via EP1 signaling in PVN-CRH neurons. (C) Under basal conditions: The equilibrium potential of GABA (E_{GABA}) is maintained such that $GABA_A$ signaling is inhibitory. GABA binding to the $GABA_A$ receptor (grey) triggers the influx of Cl^- (orange) down its electrochemical gradient hyperpolarizing the membrane potential. Neurons maintain the Cl^- gradient and thus E_{GABA} via processes involved in Cl^- homeostasis (purple). (D) In the presence of PGE2: PGE2 binding to the EP1 receptor (Green) disrupts the neuronal maintenance of intracellular chloride concentration $[Cl^-]_i$. This triggers the buildup of $[Cl^-]_i$, a depolarizing shift in E_{GABA}, and Cl^- efflux on $GABA_A$ opening. This triggers weakened, or even excitatory, GABA signaling. EP1 is a G_q couple receptor. Other G_q coupled receptors in the PVN-CRH neurons have been linked to altered Cl^- homeostasis and depolarizing shifts in E_{GABA} [65].

Rationale

There are several lines of evidence pointing to the roles of EP1 in the excitation of PVN-CRH neurons via GABA synapse plasticity. First, genetic knockdown of EP1 receptor impaired HPA axis response to inflammation [91] (FIG 1 B). Second, *in situ* hybridization and immunohistochemistry showed the postsynaptic localization of EP1 on PVN-CRH neurons [91,98] (FIG 1 B). Third, the downstream signaling pathways of EP1 – that is, the G_q-Ca^{2+} pathway [90,93] – have been directly linked to the modulation of E_{GABA}. As discussed in "GABA as a regulator of the stress response" [65,93,101], Cl^- homeostasis is one key mechanism underlying the plasticity of GABAergic synaptic transmission onto PVN-CRH neurons [41,47,65,68]. Taken together, the general hypothesis of my thesis is as follows:

Hypothesis

PGE2 changes $GABA_A$ receptor reversal potential via EP1 signaling in PVN-CRH neurons.

Aims

To test the hypothesis, we will address the following aims:

1. Using gramicidin-based perforated patch protocol (see methods), measure E_{GABA} in PVN-CRH neurons before and after PGE2 application.
2. Using whole-cell patch clamp recordings, measure E_{GABA} in PVN-CRH neurons before and after PGE2 application.
3. Investigate the contribution of EP1 in mediating PGE2-induced E_{GABA} shift. Using an EP1 agonist, and an EP1 antagonist paired with PGE2

Chapter 2

Methods and Materials

Animal Handling

All experiments using animals were approved by the Animal Care Committee at the University of Western Ontario and in compliance with Ontario Animals for Research Act. All efforts were made to minimize the number of animals used and their suffering. Experiments were performed using 60-90 day old male CRH-tdTomato reporter mice. The CRH-tdTomato mice are obtained from an in-house C57BL/6 background crossbred homozygous CRH-IRES-Cre driver (Jackson Laboratories, stock #: 012704) and a homozygous Cre-dependent ROSA26-tdTomato reporter (Jackson Laboratories, stock #: 007914). Animals were housed in cages of 3-4 cohorts. Cages consisted of bedding and a small, red-tinted shelter for environmental enrichment. Food and water were available as needed.

Slice preparation

Immediately following sacrifice, the whole brain was extracted and placed in ice-cold (~3C) slicing solution consisting of (NaCl 87 mM, KCl 2.5 mM, $NaHCO_3$ 25 mM, $CaCl_2*2H_2O$ 0.5 mM, $MgCl_2*6H_2O$ 7 mM, $NaH_2PO_4+H_2O$ 1.25 mM; glucose $C_6H_{12}O_6$ 25 mM, sucrose $C_{12}H_{22}O_{11}$ 75 mM, Osmolarity 320 mOsm, bubbled for 20 minutes). 250uM coronal slices were prepared using a vibratome (VT1200s, Leica Biosystems). The paraventricular nucleus was isolated by landmarking the anterior commissure and taking up to 1250uM slices posterior to this. For patch slice preparation, the vibratome was set to slice at 10 mm/s with a spread of 20 mm. Following slice production, the slices were cut medially along the longitudinal axis. To ensure the slices would fit in the perfusion chamber, excess tissue (primarily the cortical regions) dorsally and laterally to the PVN were cropped. The prepared slices were placed in a warmed ($34^{\circ C}$) ACSF (NaCl 125 mM, KCl 2.5 mM, $NaHCO_3$ 26 mM, $CaCl_2*2H_2O$ 2.5 mM, $MgCl_2*6H_2O$ 1.5 mM, $NaH_2PO_4+H_2O$ 1.25 mM; glucose $C_6H_{12}O_6$ 10 mM, Osmolarity 300 mOsm, bubbled for 30 minutes before use and continuously thereafter) bath (Lauda, E100 Ecoline Staredition) and held for 1 hour. Immediately following this period, the slices were removed from the warm bath (in the incubator) and allowed to warm up to room temperature (20-25C) before patch-clamp experiments.

Electrophysiology

Patch-clamp electrophysiology experiments were performed using the setup described in TABLE 1. During the experiment, slices were placed into a Warner Instruments RC-22C slice chamber and constantly perfused with warm ACSF (32C). To isolate GABAergic signaling, the AMPA and Kainate receptor antagonist 6,7-Dinitroquinoxaline-2,3-dione (DNQX) was added to the perfused ACSF (DNQX; 10 μM, from 50 mM stock dissolved in DMSO, Tocris Bioscience, CAT no. 0189, CAS: 2379-57-9). The location of the paraventricular nucleus was determined by locating the dorsal tip of the third ventricle and verifying the presence of CRH+ neurons under fluorescence at 10x magnification. Once the location of the PVN was verified, the slice was anchored in the slice chamber using custom-crafted platinum slice weights.

CRH+ positive neurons were located at 40x magnification using fluorescence. Following localization, the patch pipette was lowered towards the targeted neuron. Immediately before entering the slice, a small positive pressure was applied to the pipette, and the pipette offset was compensated for. Next, a gigaseal was achieved between the patch pipette and the targeted neuron, and pipette capacitance was compensated for. Cells that did not form a gigaseal (>1 gOhm) were discarded. In puff experiments, during the gigaseal stage, the 'puff' pipette would be placed approx. 20-60um downstream from the targeted cells.

In whole-cell patch-clamp experiments, whole-cell was achieved by applying a brief-strong- inwards suction via the mouth. Immediately following the breakthrough, cell health was monitored by applying a small voltage pulse (+5 mV) while holding the cell at -70 mV. Cells which did not achieve an access resistance below 20 mOhm or had a membrane resistance below 500 mOhm were discarded. Cells which failed to meet these criteria at any point during an experiment were excluded from analysis. All recordings were sampled at 20kHz. For voltage-clamp experiments, a Bessel filter of 1.6 kHz was applied in multi-clamp commander. For current-clamp experiments, a Bessel filter of 10 kHz was applied in multi-clamp commander. Finally, the electrophysiological identity of the cell was confirmed to be parvocellular using a brief current clamp protocol. First, a holding current (-30 to 30 pA) was applied to adjust the resting membrane potential to approximately 70 mV. Next, a small hyperpolarizing current (-20 pA) is applied prior to a ladder of depolarizing current (-20 pA - 120 pA; 20 pA steps). The voltage response waveform was used to identify the cell type by sight based on the principles

introduced in [102]. Our whole-cell internal solution consisted of K_2ATP 4 mM, Na_3GTP 0.3 mM, K-Gluconate 116 mM, KCl 8 mM, Na-Gluconate 12 mM, K_2-EGTA 1 mM, HEPES 10 mM, $MgCl_2$. Our solutions generated a junction potential of 15 mV (whole-cell) and 3.6 mV (perforated-patch), which were not compensated for in the reported results.

In gramicidin perforated patch experiments, a similar procedure to above was repeated. The patch pipette was filled with a high CL^- solution in combination with the antibiotic gramicidin (KCl 150 mM, HEPES 10 mM, osmolarity 310 mOsm, ph 7.2; 40 µg/ml Gramicidin [Sigma-Aldrich-G5002; CAS: 1405-97-6]), as outline previously [65]. This solution allowed prompt monitoring of perforated patch breakthrough. Due to the high Cl^- concentration, a breakthrough would result in a rapid depolarization of E_{GABA} to values > -15 mV [65]. Therefore, recordings that showed an of E_{GABA} > -15 mV were assumed to have a compromised perforated patch and were discarded.

The previously termed 'puff' protocol was the primary method used to measure the $GABA_A$ mediated Cl^- reversal potential during all experimental methods. In sum, the $GABA_A$ agonist muscimol (10 µM; from 100 µM stock dissolved in H_2O, Tocris Bioscience CAT no. 0289, CAS: 2763-96-4) was applied focally through the 'puff' pipette using brief air pressure (picospirtzer II; 10 ms; 10 psi). To assess the Cl^- reversal potential, the cell was held in voltage-clamp at varying holding potentials (-90 to -30 mV; 10 mV increments). The resulting membrane current from each puff was recorded (FIG 2A-B). In order to account for slight variations in current response, each holding step was repeated 5 times, and the averaged response was used for analysis (see patch-clamp analysis).

To assess the change in Cl^- reversal potential under various conditions, drugs were bath applied via a gravity-based perfusion system (See TABLE 2 for concentrations). To account for changes induced in reversal potential by technical limitations (see discussion), two different primary methodologies were used prior-to- and subsequent-to- drug application in whole-cell patch-clamp:

> **Within Cell:** In this procedure, the same cell was used for reversal potential analysis throughout the protocol. Following cell breakthrough (see above), the initial reversal potential would be measured. Subsequent to bath application of the drug, the reversal potential of the same cell would be measured periodically (5 min intervals) for up to 60

min post-drug application. In between each puff protocol, the cell health would be monitored for changes in membrane or access resistance.

Between Cells: In this procedure, multiple cells were patched prior to and following drug application. This procedure was introduced in attempt to account for technical error caused by long-term patch-clamp of cells [103]. Prior to drug application, at least three cells were patched to assess the basal reversal potential. Following drug application, cells were patched randomly and periodically to assess changes in reversal potential. Cells were only held long enough to verify cell identity and measure a single reversal potential.

Equipment Description	**Make/Model (Company)**
Microscope	Olympus BX51WI (Olympus)
Microscope Camera	IR-2000 (DAGE-MTI)
LED system	X-Cite Series 120Q (Lumen Dynamics)
Amplifier	Multiclamp Commander 700B (Molecular Devices)
Digitizier	Digidata 1440A (Molecular Devices)
Micromanipulator (patch pipette)	MP-225 (Sutter Instrument Company)
Micromanipulator (puff pipette)	Burleigh PCS-6000 (EXFO Lifesciences)
Bath Temperature Control	TC-324B (Warner Instruments Co.)
Bath Slice Chamber	RC-22C (Warner Instruments Co.)
Air Table	Vibraplane 5702E-3036-31 (Kinetic Systems)
Pipette Puller	P1000 (Sutter Instrument)

TABLE 1 – Equipment models used in patch-clamp electrophysiology experiments

Drug	Company	Stock	Final Concentration
PGE_2	Caymen Chemcial, CAT No. 14010, CAS: 363-24-6	in 5 mM stock dissolved in EtOH	1 μM
EP_1 Agonist (iloprost)	Caymen Chemical, CAT No. 18215, CAS: 78919-13-8	in 1 mM stock dissolved in EtOH	1 μM
EP_1 Antagonist (GW 848687X)	Caymen Chemical, CAT Item No. 10010410, CAS: 612831-24-0	in 2.5 mM stock dissolved in DMSO	1 μM

Vehicle (90% EtOH)	n/a	n/a	0.01% EtOH dilution or ~1 μM

TABLE 2 – Drugs bath applied during patch-clamp electrophysiology experiments

Patch-Clamp Analysis

Determination of $[Cl^-]_i$

Currents from the $GABA_A$ receptor are mediated primarily by the movement of Cl^-, and HCO_3^- across the membrane [49]. Including the role of HCO_3^- we can describe the simplified relationship between Cl^- and the $GABA_A$ current as [49,104]:

$$I_{GABA} = g_{GABAA}(V_m - E_{GABA})$$

Whereas the $GABA_A$ induced current I, is proportional to the conductance of the channel and driving force of Cl- g multiplied by the difference between the membrane potential V and the equilibrium (reversal) potential of $GABA_A$ (E_{GABA}). E_{GABA} itself is determined by the Cl^-, and HCO_3^-. To this end, the equilibrium potential of $GABA_A$ across the membrane is determined partially by two factors (1) the concentration of Cl^- and HCO_3^-, on either side of the membrane, (2) other anion concentrations. Excluding #2 based on its weak contribution to this drive [105]; we can describe the relationship between (1) and equilibrium potential by the simplified Goldman-Hodgkin-Katz equation [104]:

$$E_{GABA} = \left(\frac{RT}{F}\right) log\left(\frac{4[CL-]_o + [HCO_3-]_o}{4[CL-]_i + [HCO_3-]_i}\right)$$

Where R is the universal gas constant, T is the temperature in kelvin, F is the faraday constant, and $[CL-]_o, [HCO_3-]_o$ & $[CL-]_i, [HCO_3-]_i$ are the ionic concentrations outside and inside the cell, respectively. Experiments were completed under the assumption that $[CL-]_o, [HCO_3-]_o$ was consistent across spatial and temporal space. With this in mind, we can compute our theoretical E_{GABA} based on our known ionic composition. Given that E_{GABA} is proportional to -in part- $[Cl^-]_i$, we utilized E_{GABA} as a proxy for measuring changes in internal Cl^- concentration.

Patch Method	Cl^- Concentration		HCO_3^- Concentration		Theoretical E_{GABA} (mV)
	$[Cl^-]_i$	$[Cl^-]_o$	$[HCO_3^-]_i$	$[HCO_3^-]_o$	
Whole Cell	12	136.5	0	26	-64.97
Perforated	150	136.5	0	26	1.44

TABLE 3 – Theoretical E_{GABA} based on known internal and external ionic composition

Statistical Analysis

E_{GABA} was computed from the recorded 'puff' voltage-clamp traces (see methods - electrophysiology). To do so, the five sweeps for each holding potential were averaged to account for noise in the recording. Then, the maximal absolute current amplitude for each holding potential was calculated. The maximal absolute current amplitude was found with a search area of up to 1 second following puff (10 ms) application.

Next, the data was organized such that each current (y; dependent variable), was paired with holding potential (x; independent variable). Then, the data was fit with simple linear regression in the form of (FIG 2C):

$$y_{current} = mx_{potential} + b$$

Where y represents the absolute maximal current at holding potential x. m is the slope of the line. b represents the y-intercept of the line. The data was fit using the ordinary least squares method. In this formulation, E_{GABA} is the holding potential at which there is no net current, thus represented by the x-intercept (FIG 2C). The x-intercept was calculated by setting y to 0 and proceeding as follows:

$$0 = mx_{potential} + b$$

$$x_{potential} = \frac{0-b}{m}$$

Or alternatively:

$$E_{GABA} = \frac{0 - b}{m}$$

The computed E_{GABA} was used for follow-up analysis. Each recording was independently fit with linear regression and E_{GABA}. For each recording, the linear fit was confirmed to have a significantly non-zero slope, otherwise the data was discarded.

In some cases, we desired to pool cell data prior to fitting with linear regression. However, we observed recording-to-recording differences in current amplitude arising from intrinsic differences in cell size, receptor expression, and puff pipette localization. Such differences in current amplitude may skew the resulting averaging and linear fit. To account for

this, in these analyses, the current was scaled to the range of [-1,1] by the maximum absolute value. This can be expressed as:

$$I_{current} = \frac{I_{Current}}{max(abs(I))}$$

Where $I_{current}$ represents a single current point. I represents the full set of current points for that recording. $max(\ \ )$ and $abs(\ \ )$ represent the maximum and absolute functions respectively. Each recording was scaled independently prior to pooling.

Data was grouped by treatment and time for follow-up analysis. Follow-up statistical analysis was completed with a two-way ANOVA (treatment x time) wherever possible. Tukey's multiple comparisons were utilized as post-hoc analysis. Due to challenges associated with the long recording time (>30 minutes) destabilizing cell health (in both gramicidin and whole-cell conditions) [103,106,107], some cells failed to reach the full recording length. Therefore, we were unable to use a repeated measures two-way ANOVA due to constraints with missing values. For time-course analysis, data was baselined on a per cohort basis to account for intrinsic differences between subjects and cells. Otherwise, a student's unpaired t-test or one-way ANOVA was used. For reporting, a p-value <0.05 was considered significant.

Software Used

MultiClamp Commander software (Molecular devices) was used for amplifier control and filtering. Protocol design and recordings were completed using the Clampex software Clampex 10.7, pClamp, Molecular devices). Averaging and calculation of maximal current amplitude was completed using the Clampfit software (Clampfit 10.7, pClamp, Molecular devices).

Linear regression, computation of E_{GABA}, data scaling, and other statistical analyses were completed using GraphPad Prism 8 (GraphPad Prism 8.3.1 (549), Graphpad Software, LLC). Figures were generated using GraphPad Prism 8, and Adobe Illustrator CC 2020 (Adobe Illustrator CC 2020 24.3, Adobe Software). Writing was completed using Microsoft Word (Microsoft Word 18.2106.12410.0, Microsoft Corporation). References were managed and inset

using Mendeley, and the Mendeley Microsoft Word Software plugin (Mendeley Desktop 1.19.3, Mendeley LTD, Elsevier).

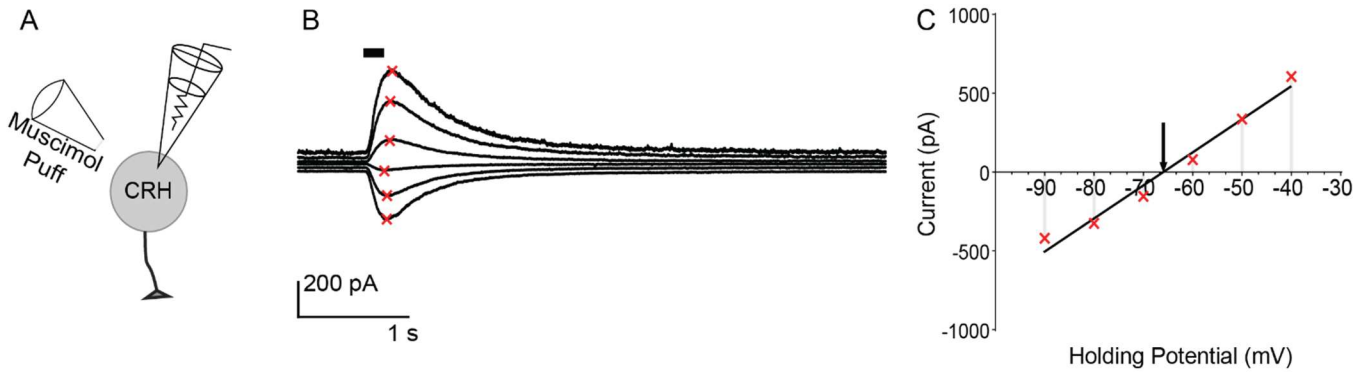

FIG 2 – The assessment of E_{GABA} using patch-clamp electrophysiology and focal application of a $GABA_A$ receptor agonist Muscimol

(A) Schematic representation of patch-clamp recording configuration. The whole-cell or perforated patch clamp is achieved in a CRH neuron. To activate the postsynaptic $GABA_A$ receptors, muscimol (10 μM) is focally applied using air pressure (10 ms) from a glass pipette placed approximately 30-60 μm from the soma of the recording neuron. (B). A representative voltage-clamp trace. The cell is held at different membrane potentials to assess the peak amplitude and direction of the muscimol-induced current. Each line represents a different holding potential ranging from -90 mV (bottom) to -40 mV (top). The black bar indicates the application of a 10 ms muscimol puff. Each red X represents the points at which the maximum absolute current was observed. (C) The extrapolated I-V relationship was generated from the patch-clamp recordings. Each red X indicates the absolute maximum current found after the puff. The black line shows the least-squares linear regression fit to the data (R^2: 0.9925; $p < 0.0001$). The x-intercept (-66.40 mV) represents the reversal potential for $GABA_A$ receptor-mediated current in this neuron (black arrow).

Chapters 3

Results

PGE2 induces a depolarizing shift in E_{GABA}

We hypothesize that PGE2 causes a depolarizing shift in E_{GABA}, which results in a loss of GABAergic inhibition. To test this, we measured the E_{GABA} before and after PGE2 (1 μM) application using the perforated patch-clamp technique (see methods). Briefly, we held the post-synaptic membrane potentials at various levels and recorded $GABA_A$ receptor-mediated currents by focally applying muscimol (10 μM), a specific agonist for $GABA_A$ receptors (Fig. 2A). We then plotted the maximal (peak) current response (I) as a function of the holding-membrane potential (V); the resulting function was fit with linear regression to extrapolate the E_{GABA}. We found that E_{GABA} was -78.86 ± 7.50 mV (n=14) under the basal conditions with the perforated patch approach. This is consistent with previous findings in rats and mice [65,66].

In a subset of neurons, E_{GABA} was repeatedly measured at 10-minute intervals during the baseline (-10 and 0 min) and after drug (PGE2 or drug) applications (10-60 min). Fig. 3B shows that PGE2 caused a depolarizing shift in E_{GABA}, which was time-dependent and reversible after the washout of PGE2. On the other hand, vehicle (0.01% EtOH) caused no change. The baseline E_{GABA} was not significantly different between PGE2 and vehicle groups (PGE2 baseline n=7, VEH baseline n=7, Tukeys's; DF=50; PGE2 baseline vs VEH baseline q=0.9791, p=0.8896; see below). A two-way ANOVA revealed a significant interaction between treatment x time and the main effects of treatment but not time (n=65; Treatment X Time: $F(6, 51) = 5.949$, $p<0.0001$, Treatment: $F(1, 51) = 52.22$, $p<0.0001$; Time: $F(6, 51) = 1.130$, $p=0.3582$). Post-hoc analysis showed a significant difference between baseline (T=-10) and the 10–30-minute time points in the PGE2 condition (n=7 for all; Tukey's; DF=51; -10 vs 10: $q=5.032$, $p=0.0135$; -10 vs 20: $q=6.921$, $p=0.0002$; -10 vs 30: $q=5.339$, $p=0.0072$). In contrast, the vehicle control condition showed no significant difference between any time points (n=5 for all; Tukey's; DF=51; $q<2.5$ for all; $p>0.5$ for all). We also found that E_{GABA} was significantly higher in PGE2 than vehicle at time points between 10 and 30 min (n=7 for PGE2, n=5 for VEH; Tukeys's; DF=51; -10 PGE2 vs -10 VEH: $q=0.0899$, $p>0.9999$; 10 PGE2 vs 10 VEH: $q=5.410$, $p=0.0218$; 20 PGE2 vs 20 VEH: $q=8.992$, $p<0.0001$; 30 PGE2 vs 30 VEH: $q=6.194$, $p=0.0042$).

The time-course measurement of E_{GABA} indicated that the PGE2-induced E_{GABA} shift becomes evident anytime between 10 and 30 min after the drug application. Thus, we pooled additional cells whose E_{GABA} was measured at a single time point between 10-30 minutes after the drug application to compare pre- and post-drug E_{GABA} changes. Fig. 3C shows the pre- and post-drug I-V curves for PGE2 and vehicle treatments. The I-V curves were normalized per-cell to a range of [-1,1] to account for the cell-to-cell variability in the absolute current amplitude (this is primarily due to technical variability arising from the relationship between GABA applying pipette and the recorded neurons; see methods). The normalization allows averaging across cells without disrupting slope or x-intercept (see methods). We then compared the resulting linear regressions for the three conditions (the baseline, post-PGE2, post-vehicle). The linear regression for each condition was significantly non-zero (simple linear regression; Baseline: $F(1,64)=56.62$, $p<0.0001$; PGE2: $F(1,28)=39.73$, $p<0.0001$; VEH: $F(1, 10)=18.65$, $p=0.0015$). The slope between each condition was not significantly different between groups, indicating that PGE2 does not change the whole-cell $GABA_A$ receptor conductance. On the other hand, the intercepts were significantly different from each other (ANCOVA; slope: $F(2,102)=0.6306$, $p=0.5343$; intercept: $F(2, 104)=20.68$, $p<0.0001$), indicating PGE2-induced an E_{GABA} shift.

In the pooled data, a two-way ANOVA revealed a significant interaction between treatment and time (two-way ANOVA; n=54; Time x Treatment: $F (1, 50) = 18.90$, $p<0.0001$; Time: $F (1,50)=4.646$, $p=0.0360$; Treatment: $F (1,50)=9.980$, $p=0.0027$) (Fig. 3 D compares E_{GABA} for pre- and post-drug application for PGE2 and vehicle). The baselines and VEH conditions were not significantly different from each other, but both significantly different from the PGE2 condition (PGE2 baseline n=7, VEH baseline n=7, PGE2 n=23, EtOH n=17; Tukeys's; DF=50; PGE2 baseline vs VEH baseline $q=0.9791$, $p=0.8896$; PGE2 10-30 minute vs VEH 10-30 minute, $q=10.34$, $p<0.0001$; PGE2 baseline vs PGE2 10-30 minute, $q=6.635$, $p=0.0001$; VEH baseline vs VEH 10-30 minute, $q=2.150$, $p=0.4334$). The mean shift between the PGE2 baseline and pooled 10–20-minute data was -24.92 ± 5.31 mV (-78.86 ± 7.50 mV, n=7; -56.22 ± 13.49 mV, n=23; respectively).

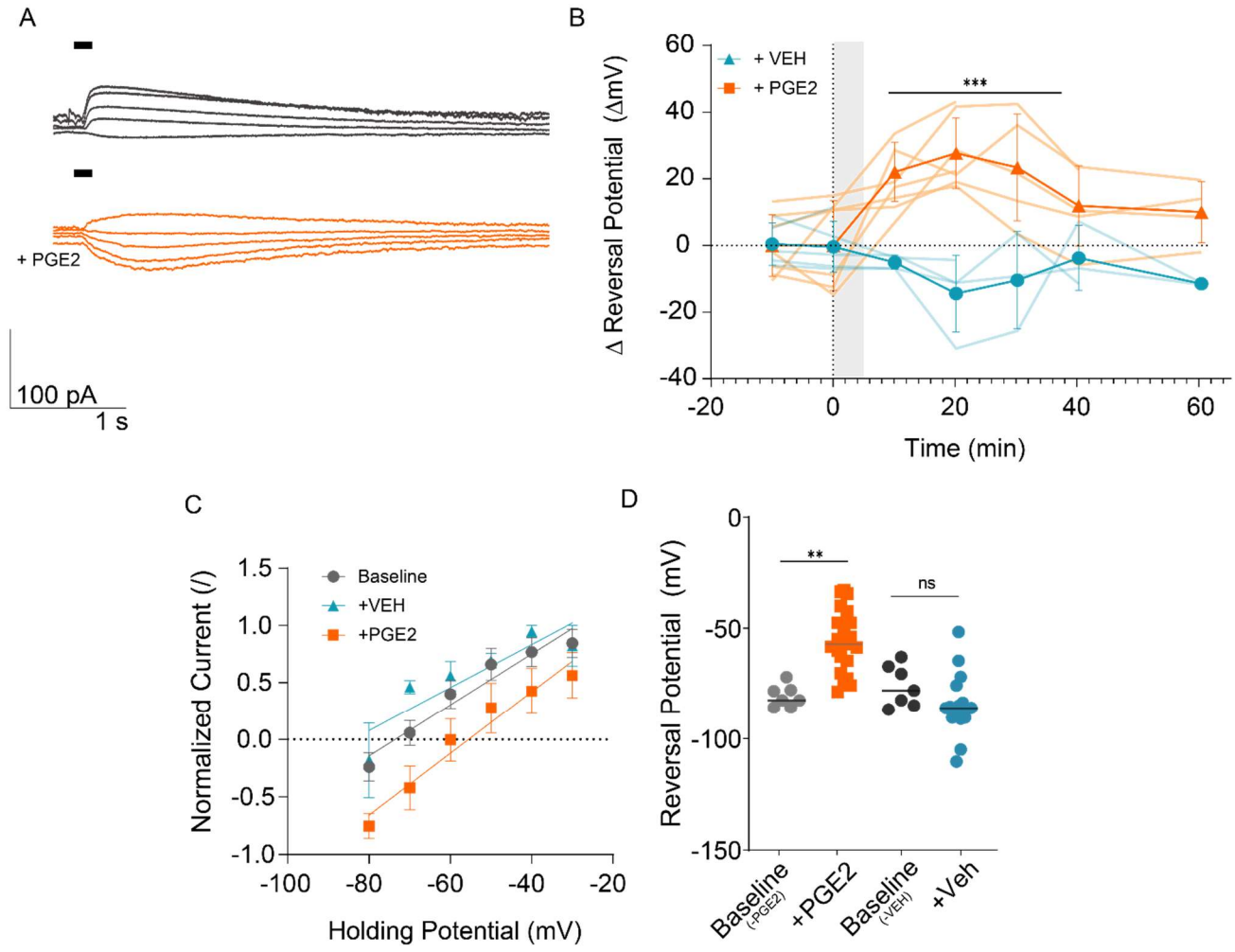

FIG 3 – PGE2 induces a time-dependent shift in E_{GABA}.

(A) Representative voltage-clamp trace showing a single unit response to muscimol puffs (black bar; 10ms) pre- (top, grey) and post- (bottom, orange) PGE2 application. Each trace represents a different holding potential ranging from -70 mV (bottom) to -30 mV (top). (B) A plot of the measured reversal potential in respect to time and condition. Application of drug (PGE2 [Orange], VEH [Blue]) occurs at time point 0 (dotted line) and lasts five minutes (grey overlay), subsequently the drug is washed out. Baseline data recorded at -10min. A two-way ANOVA revealed a significant interaction between treatment x time (n=65; Treatment X Time: $F(6, 51) = 5.949$, $p<0.0001$, Treatment: $F(1, 51) = 52.22$, $p<0.0001$; Time: $F(6, 51) = 1.130$, $p=0.3582$). In the PGE2 condition, post-hoc analysis showed a significant difference between the -10 minute, and 10–30-minute time points (n=7 for all; Tukey's; DF=51; -10 vs 10: q=5.032,

p=0.0135; -10 vs 20: q=6.921, p=0.0002; -10 vs 30: q=5.339, p=0.0072) (C) I-V relationship for each condition. Current amplitude is normalized to [-1,1] for each neuron, and then the average is computed for each condition. The intercept represents E_{GABA} of each condition and are higher in PGE2 than the baseline or VEH (ANCOVA; intercept: F(2, 104)=20.68, p<0.0001). On the other hand, the slopes, which reflect the postsynaptic total $GABA_A$ receptor conductance, were similar between the baseline, VEH and PGE2 (ANCOVA; slope: F(2,102)=0.6306, p=0.5343). (D) Plot of the recorded reversal potential for each condition. Each point represents a single measure. The VEH and PGE2 conditions represent data pooled from points recorded in the 10–30-minute conditions (see results). A two-way ANOVA revealed a significant interaction between treatments and time (two-way ANOVA; n=54; Time x Treatment: F (1, 50) = 18.90, p<0.0001; Time: F (1,50)=4.646, p=0.0360; Treatment: F (1,50)=9.980, p=0.0027). The baselines and VEH conditions were not significantly different from each other, but both significantly different from the PGE2 condition (PGE2 baseline n=7, VEH baseline n=7, PGE2 n=23, VEH n=17; Tukeys's; DF=50; PGE2 baseline vs VEH baseline q=0.9791, p=0.8896; PGE2 10-30 minute vs VEH 10-30 minute, q=10.34, p<0.0001; PGE2 baseline vs PGE2 10-30 minute, q=6.635, p=0.0001; VEH baseline vs VEH 10-30 minute, q=2.150, p=0.4334). ***, p<0.015. ns (not significant), p>0.05

Whole-Cell Patch-Clamp effectively detects PGE2-induced E_{GABA} shift

Gramicidin perforated patch-clamp is a commonly used approach to measure E_{GABA} because it forms pores impermeant to Cl^- and thus does not disrupt the cell-intrinsic intracellular Cl^- composition [108]. On the other hand, whole-cell patch-clamp techniques allow the intracellular cytosol to become continuous with the artificial intracellular solutions in the patch pipette, which alters the cell-intrinsic intracellular Cl^- composition [108]. However, whole-cell patch-clamp is an important alternative because whole-cell configuration allows us to apply various drugs through the recording pipette to dissect intracellular signaling mechanisms that lead to altered post-synaptic Cl- homeostasis. In addition, whole-cell is superior to perforated patch-clamp for the control of the postsynaptic membrane potential, and as a consequence, the measurement of E_{GABA}. Importantly, a number of previous studies have effectively used whole-cell configuration to measure E_{GABA} changes induced by pharmacological manipulations as well as behavioural manipulations [65,68,109,110]. This was possible because E_{GABA} reflects a dynamic balance between the activities of Cl^- pumps (KCC2 and NKCC1) and Cl^- channels ($GABA_A$ receptors and other Cl- channels) that constantly exchange Cl^- across the membrane. Thus, any changes in the dynamic Cl^- balance (e.g. Cl^- pump activities) will shift the E_{GABA} even under the whole-cell configuration [68].

Using the whole-cell patch-clamp approach, we found, in basal conditions, a mean E_{GABA} of -57.42 ± 4.59 mV, representing a shift of 21.44 mV compared to the perforated patch baseline. The depolarized E_{GABA} is in line with the predicted E_{GABA}: -64.97 mV, based on the $[Cl-]_o$, $[HCO_3^-]_o$ and [Cl-]i, $[HCO_3^-]_i$ we used in the experiment. This is congruent with previously reported values taken in whole-cell experiments [65,68].

To examine PGE2-induced E_{GABA} shift, E_{GABA} was measured before and at various time points after PGE2 application up to 60 min (Fig. 4 A). Some neurons were repeatedly measured before and several time points after PGE2 (1 μM) application, whereas some other cells were measured only at a single time point (see methods). Similar to the perforated-patch configuration, we found a time-dependent shift in E_{GABA} following the application of PGE2 (Fig. 4 B). A two-way ANOVA revealed a significant interaction between treatment x time (two-way ANOVA; n=75; Treatment, $F(1, 62)=54.45$, $p<0.0001$; Time, $F(6,62)=2.831$, $p=0.0168$; Time x Treatment, $F(6,62)=5.763$, $p<0.0001$). Post-hoc analysis of the PGE2 condition showed a

significant difference between the -10 minute and 20 & 60 minute time points (Tukey's; n=5; DF=62; -10 vs 20: q=5.285, p=0.0071, -10 vs 60: q=8.202, p<0.0001), and a significant difference between 0 minute and 20 – 60-minute conditions (Tukey's; n=5; DF=62; 0 vs 20: q=5.456, p=0.0049, 0 vs 30: q=4.440, p=0.0393; 0 vs 40: q=4.744, p=0.0219; 0 vs 60: q=7.409, p<0.0001). However, the -10 min condition was not significantly different from the 30–40-minute conditions (Tukey's; n=5, DF=62, -10 vs 30: q=3.672, p=0.1449; -10 vs 40: q=4.048, p=0.0792). In contrast, post-hoc analysis of the VEH condition showed no significant difference for any time points (Tukey's; n=5; DF=62; q<2.6, p>0.5 for all). These data indicated that, in the whole-cell configuration, the PGE2-induced E_{GABA} shift becomes evident between 20-40 min after drug application.

In order to compare pre- and post-drug conditions, we pooled the data from the 20-40 min bins for further analysis. We assessed the I-V relationship for the baseline and PGE2 conditions (Fig. 4 C). The slope of the line was significantly non-zero for all conditions (simple linear regression; Baseline: F(1,56)=123.4, p<0.0001; PGE2: F(1,28)=213.6, p<0.0001). Similar to the perforated patch experiments, the slopes between baseline and PGE2 did not significantly differ; however, the intercepts did (ANCOVA; slope: F(1,111)=0.2028, p=0.6533; intercept: F(1, 112)=19.08, p<0.0001).

After pooling the data, a two-way ANOVA revealed a significant interaction between treatment x time (two-way ANOVA; n=91; Treatment: F(1,87)=17.28, p=<0.0001; Time: F(1,87)=17.46, p<0.0001; Treatment x Time: F(1,87)=15.04, p=0.0105). A post-hoc analysis showed that the PGE2 and VEH condition baselines did not differ, but the 10-30 min time-points did (FIG 4 D)(PGE2 baseline n=30, VEH baseline n=13, PGE2 treatment=30, VEH treatment=18; Tukey's; DF=87, Baseline PGE2 vs Baseline VEH: q=1.464, p=0.7293; 10–30-minute PGE2 vs 10 -30 minute VEH: q=7.169, p<0.0001). The PGE2 condition showed a mean depolarizing shift of -7.55 ± 1.28 mV compared to its respective baseline (n=30, n=30; Tukey's; DF=87; q=8.304, p<0.0001). The VEH control condition did not differ from its respective baseline (n=13, n=18; Tukey's; DF=87; q=1.365, p=0.7736). Similar to the baseline, the whole-cell PGE2 condition and perforated patch PGE2 conditions showed a significant difference, with a mean shift of -6.751 ± 2.695 (unpaired t-test; whole cell n=30, perforated patch n=22; t=2, whole-cell PGE2 mean -49.47 ± 5.71 mV vs perforated-patch PGE2 mean -56.22 ± 13.49 mV).

In summary, we validated that whole-cell configuration is effective in detecting PGE2-induced E_{GABA} shift, as has been shown by other studies [65,68].

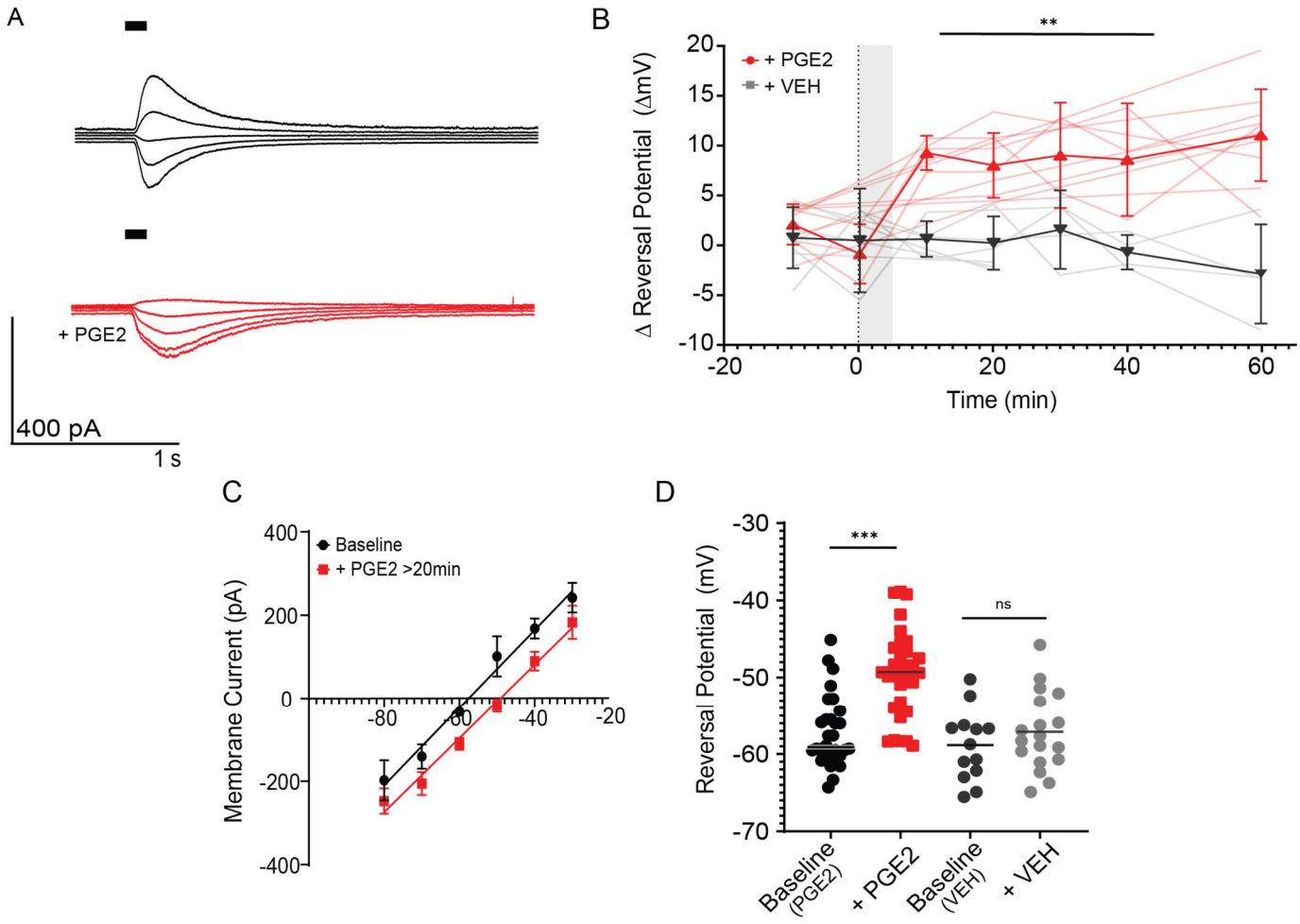

FIG 4 – PGE2-induced E_{GABA} shift measured by whole-cell patch clamp recordings

(A) Representative voltage-clamp trace showing a single unit response to muscimol puffs (black bar) pre- (top, black) and post- (bottom, red) PGE2 application. Each trace represents a different holding potential ranging from -70 mV (bottom) to -30 mV (top). (B) Scatter plot of the change in reversal potentials measured across time for the post-PGE2 (red) and VEH (grey) conditions. Application of drug occurs at time point 0 (dotted line) and lasts five minutes (grey overlay), subsequently the drug is washed out. A two-way ANOVA showed a significant interaction between treatment x time (two-way ANOVA; n=75; Treatment, $F(1, 62)=54.45$, $p<0.0001$; Time, $F(6,62)=2.831$, $p=0.0168$; Time x Treatment, $F(6,62)=5.763$, $p<0.0001$). Post-Hoc analysis showed the t=0 time-point and 20–40-minute time points differed for the PGE2 condition (Tukey's; n=5; DF=62; 0 vs 20: $q=5.456$, $p=0.0049$, 0 vs 30: $q=4.440$, $p=0.0393$; 0 vs

40: q=4.744, p=0.0219; 0 vs 60: q=7.409, p<0.0001). (C) Mean I-V curves for pre- (black) and post- PGE2 (red) conditions. Note the 'rightwards' depolarizing shift in the I-V relationship in the post-PGE2 condition. (D) Extrapolated Cl^- reversal potentials for units under basal conditions (black, n=30, N=8), 20-40-min post PGE2 application (red, n=30, N=7), basal pre-VEH conditions (dark-grey, n=13, N=4) and 20-40-min post-VEH application (grey, n=18, N=4). A two-way ANOVA reported a significant difference interaction between treatment x time (two-way ANOVA; n=91; Treatment: F(1,87)=17.28, p=<0.0001; Time: F(1,87)=17.46, p<0.0001; Treatment x Time: F(1,87)=15.04, p=0.0105). Post-Hoc analysis revealed a significant shift in the reversal potential of the post-PGE2 condition (compared to pre-PGE2 and post-VEH conditions [PGE2 baseline n=30, VEH baseline n=13, PGE2 treatment=30, VEH treatment=18; Tukey's; DF=87, Baseline PGE2 vs Baseline VEH: q=1.464, p=0.7293; 10-30 minute PGE2 vs 10 -30 minute VEH: q=7.169, p<0.0001][n=30, n=30; Tukey's; DF=87; q=8.304, p<0.0001].) ***, p<0.0001. **, p<0.05. ns (not significant): p>0.05.

EP1 mediates the PGE2 induced shift in E_{GABA} in PVN-CRH neurons

Our working hypothesis is that PGE2 depolarizes E_{GABA} via the EP1 receptor. To test this, we bath applied the EP1 receptor agonist iloprost (1 μM) and examined E_{GABA} changes using whole-cell patch-clamp recordings. In a separate experiment, we also antagonized the EP1 receptor during the application of PGE2: specifically, we first applied the EP1 competitive antagonist (GW-848687x, 1 μM), then bath applied PGE2 (1 μM). E_{GABA} was measured before and at a single time point after the drug application. First, we examined the I-V curves for both the EP1 agonist and EP1 antagonist conditions. The slope of the baseline, EP1 conditions, and EP1 antagonist conditions were all significantly non-zero (simple linear regression; Baseline: $F(1, 56)=123.4$, $p<0.0001$; EP1: $F(1,33)=107.3$, $p<0.0001$; EP1 antagonist + PGE2: $F(1,22)=96.09$, $p<0.0001$) (Fig 5 B). The EP1 condition showed a significant difference in intercept but not slope compared to the baseline conditions (ANCOVA; slope: $F(1,89)<0.0001$, $p=0.9932$; intercept: $F(1, 90)=14.31$, $p=0.0003$). The EP1 antagonist + PGE2 condition did not show a significantly different slope or intercept when compared to controls (ANCOVA; slope: $F(1,78)=0.0003$, $p=0.9855$; intercept: $F(1, 90)=1.967$, $p=0.1647$) (Fig 5 D).

A one-way ANOVA revealed a significant effect of treatment (one-way ANOVA, n=94; Treatment: $F(3, 90)=19.55$, $p<0.0001$). Following EP1 agonist application, we observed a significant depolarizing shift in reversal potential comparable to that observed in the PGE2 condition; PGE2 mean -49.47 ± 5.76 mV vs EP1 mean -49.41 ± 3.40 mV (Tukey's; baseline n=48, PGE2 n = 31, EP1 n=8; DF=90; Baseline vs EP1: $q=6.134$, $p=0.0002$; Baseline vs PGE2, $q=10.09$, $p<0.0001$; PGE2 vs EP1: $q=0.04518$, $p>0.9999$), indicating that EP1 activation is sufficient to cause a depolarizing shift in E_{GABA} (Fig 5 A & E). PGE2 application in the presence of an EP1 antagonist did not induce a significant shift from baseline control but was different from the post PGE2 condition (Tukey's; baseline n=48, PGE2 n = 31, EP1 n=8; EP1 antagonist + PGE2 n=7; DF=90; Baseline vs EP1 antagonist + PGE2: $q=1.801$, $p=0.5819$; PGE2 vs EP1 antagonist + PGE2: $q=3.813$, $p=0.0410$; EP1 vs EP1 antagonist + PGE2: $q=3.118$, $p=0.1298$) (Fig 5 B & E). These results indicate that EP1 is necessary for the PGE2-mediated depolarizing shift in E_{GABA}.

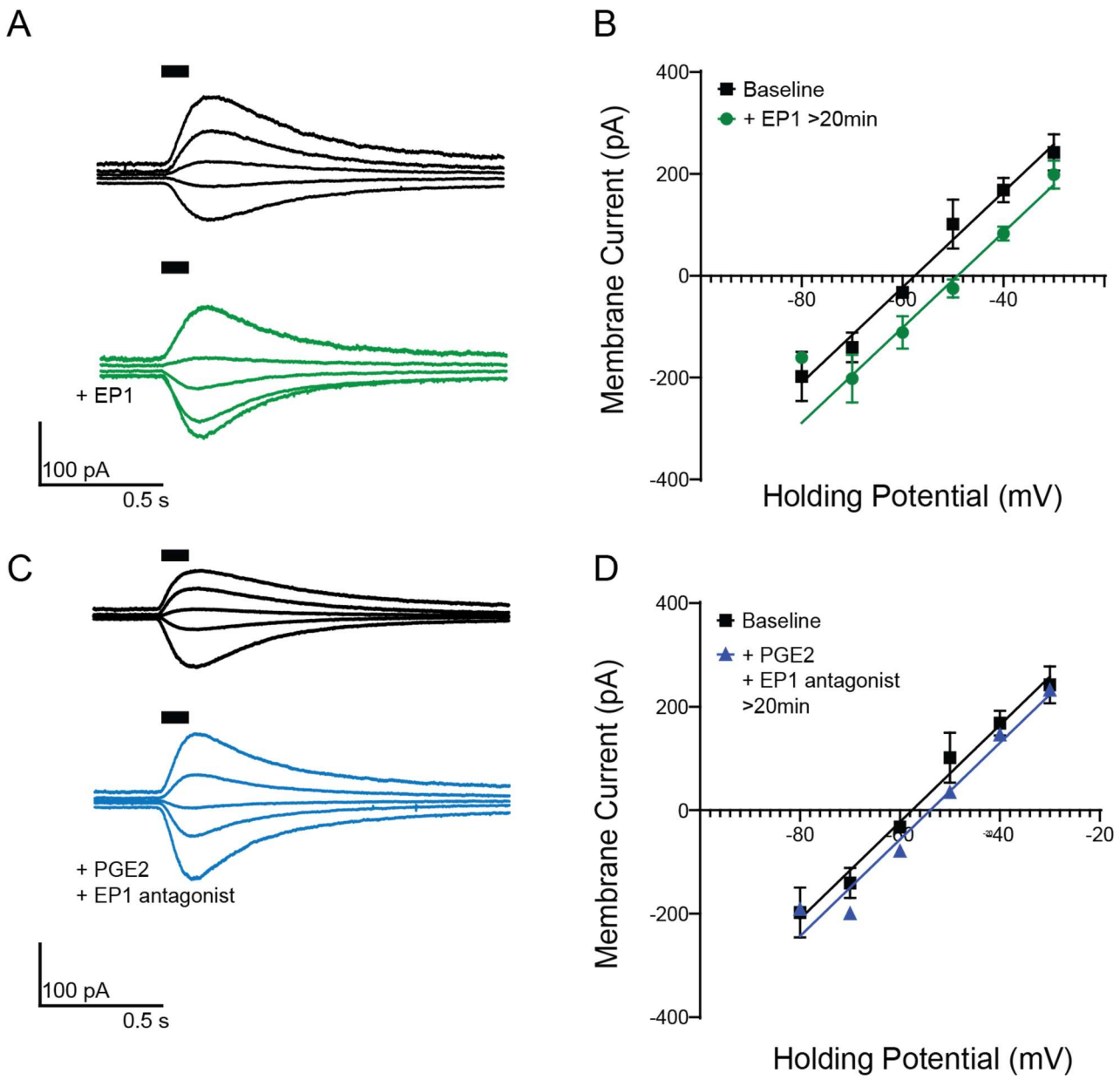
A
+ EP1
100 pA
0.5 s
B
Baseline
+ EP1 >20min
Membrane Current (pA)
400
200
0
-200
-400
-80
-60
-40
Holding Potential (mV)
C
+ PGE2
+ EP1 antagonist
100 pA
0.5 s
D
Baseline
+ PGE2
+ EP1 antagonist
>20min
Membrane Current (pA)
400
200
0
-200
-400
-80
-60
-40
-20
Holding Potential (mV)

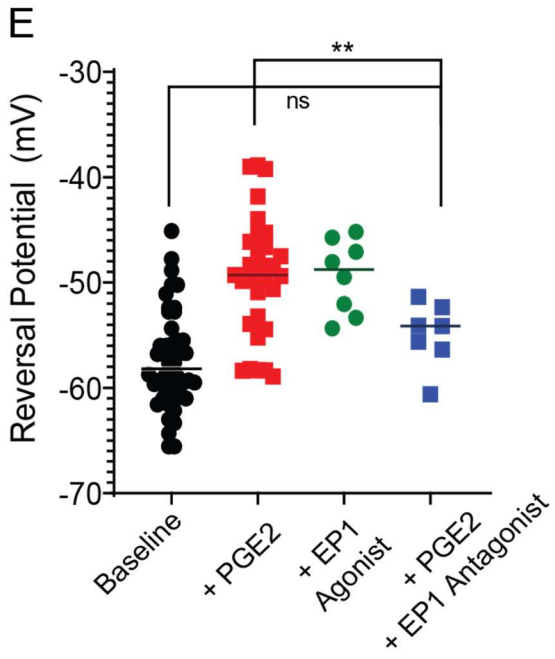
E
**
ns
Reversal Potential (mV)
-30
-40
-50
-60
-70
Baseline
+ PGE2
+ EP1 Agonist
+ PGE2 + EP1 Antagonist

FIG 5 - EP1 mediates the PGE2-induced depolarizing shift in E_{GABA}

(A) Representative voltage-clamp trace showing a single unit response to muscimol puffs (black bar) pre- (top, black) and post- (bottom, green) EP1 (iloprost 1 μM) application. Each trace represents a different holding potential ranging from -70 mV (bottom) to -30 mV (top). Note the shift in reversal potential following EP1 wash on. (B) Mean I-V trace for pre- (black) and post- (green) EP1 conditions. Note the depolarizing shift in the curve. Slopes between the two lines did not differ significantly but intercept did (ANCOVA; slope: $F(1,89)<0.0001$, $p=0.9932$; intercept: $F(1, 90)=14.31$, $p=0.0003$). (C) Representative voltage-clamp trace showing a single unit response to muscimol puffs (black bar) pre- (top, black) and post- (bottom, blue) PGE2 + EP1 antagonist (blue, GW-848687x 1 μM). Each trace represents a different holding potential ranging from -70 mV (bottom) to -30 mV (top). (D) Mean I-V trace for pre- (black) and post- (blue) PGE2-EP1 conditions. Note that the basal I-V trace occludes the post-PGE2-EP1 trace. Neither slope nor intercept differed between the two lines (ANCOVA; slope: $F(1,78)=0.0003$, $p=0.9855$; intercept: $F(1, 90)=1.967$, $p=0.1647$). (E) Extrapolated reversal potentials for basal conditions (black, n=48, N=8), 20-min post PGE2 application (red, n=31, N=7), 20-min post EP1 agonist (green, iloprost 1 μM, n=8, N=3), and 20-min post PGE2 in the presence of EP1 antagonist (blue, GW-848687x 1 μM, n=7, N=3). One-way ANOVA shows a significant difference between means (one-way ANOVA, n=94; Treatment: $F(3, 90)=19.55$, $p<0.0001$). Post-hoc analysis reveals post-PGE2 condition is significantly different from basal and PGE2+EP1 antagonist conditions, but did not differ from the post-EP1 condition (Tukey's; baseline n=48, PGE2 n = 31, EP1 n=8; DF=90; Baseline vs EP1: $q=6.134$, $p=0.0002$; Baseline vs PGE2, $q=10.09$, $p<0.0001$; PGE2 vs EP1: $q=0.04518$, $p>0.9999$; Baseline vs EP1 antagonist + PGE2: $q=1.801$, $p=0.5819$; PGE2 vs EP1 antagonist + PGE2: $q=3.813$, $p=0.0410$; EP1 vs EP1 antagonist + PGE2: $q=3.118$, $p=0.1298$). **, $p<0.05$. ns (not significant), $p>0.05$.

Chapter 4

Discussion

In this thesis, we examined the role of PGE2 and its receptor subtype EP1 in modulating E_{GABA} in PVN-CRH neurons. In aim 1, we implemented the perforated patch technique in genetically identified CRH neurons in the PVN of a well-established CRH-reporter mouse line [18]. We then observed the effects of PGE2 application on E_{GABA} in the PVN-CRH neurons. Using this technique, we found that the baseline (pre-PGE2) E_{GABA} of PVN-CRH neurons are similar to that of putative CRH neurons recorded in Sprague-Dawley rats and C57BL/6 mice [47,65,66]. We found that PGE2 caused a depolarizing shift in E_{GABA}. The result was time-dependent, becoming significant by 10 minutes after application and lasting up to 30 minutes.

In Aim 2, we sought to replicate the PGE2 experiments in whole-cell patch clamp recordings. Despite baseline differences (compared to perforated patch), we observed a similar depolarizing shift in E_{GABA} following PGE2 application. The depolarizing E_{GABA} shift lasted for more than 20 min after the washout of PGE2. Notably, in both perforated and whole-cell experiments, PGE2 did not induce a change in the slope of the current-voltage relationship of the whole-cell $GABA_A$-mediated currents. However, it did shift the intercept (i.e. E_{GABA}), indicating that PGE2 primarily changes Cl^- homeostasis and does not cause detectable changes in $GABA_A$ receptor function in the postsynaptic cells [41].

In Aim 3, we showed that EP1 agonist (iloprost) induced a slow depolarizing shift in E_{GABA}, similar to that observed in the PGE2 experiments. Congruent with this, PGE2 application in the presence of an EP1 antagonist (GW-848687x) attenuated the depolarizing shift in E_{GABA} introduced by PGE2. Collectively, our data supports the hypothesis that PGE2-EP1 signaling mediates a post-synaptic shift in E_{GABA} in PVN-CRH neurons.

PGE2 triggers a depolarizing shift in E_{GABA} in PVN-CRH neurons in perforated patch

Previous studies showed plasticity in E_{GABA} in putative PVN-CRH neurons due to various stressors [41,47,65]. These studies employed a gramicidin perforated patch technique to measure E_{GABA} in the absence of intracellular cytoplasmic disruption [65,108]. However, the noted

studies were conducted in Sprague-Dawley rats or C57BL/6 mice where definitive identification of CRHergic cell-type were not conducted [65,66]. We first sought to implement the same technique in the transgenic CRH-IRES-Cre; Ai14 mouse line. This mouse line (with a C57BL/6 background) expresses the fluorescent reporter tdTomato driven by the CRH promotor gene, thus allowing rapid, visual identification of CRH neurons in acute PVN slices. In this mouse line, applying the perforated patch technique required slight adjustment compared to the previously reported methodology. More specifically, we utilized a slightly lower concentration of gramicidin (40ug/ml) compared to the 60-50ug/ml reported in the literature [65,66]. Higher concentrations facilitated rapid break down of the cell membrane, and lower concentrations resulted in too high of an access resistance. The reasons for this modest discrepancy remain unknown. Regardless, we measured an E_{GABA} of -78.86 ± 7.50 mV in the basal condition, congruent with the previously reported values [47,65,111].

Next, we examined the time course of the effects of PGE2 on E_{GABA} in these PVN neurons. To do so, we repeatedly measured E_{GABA} in 10-minute intervals following a 5-minute wash-on of PGE2. PGE2 induced a relatively slow depolarizing shift in E_{GABA}. We observed a significant shift in E_{GABA} that onset 20 minutes after PGE2 wash on (15 minutes after washout). This effect lasted up to 40 minutes after wash-on. Grouping together the 20–40-minute conditions, we noted depolarizing shift of E_{GABA} to -56.22 ± 13.49 mV. We examined the relationship between the evoked current in response to the held membrane voltage by fitting this relationship with a simple linear regression (see methods). Importantly, the slopes between the baseline and + PGE2 conditions did not change, indicating that PGE2 does not change the whole-cell $GABA_A$ receptor conductance (e.g. potentiation of receptors, synaptic formation, etc.) [41,104,112]. Instead, the change in y-intercept indicates a shift in $E_{GABA.}$ Together the evidence points towards a mechanism of PGE2 based disinhibition of PVN-CRH neurons. That is, PGE2 induces a shift in E_{GABA} that weakens GABAergic signaling, thereby leading to disinhibition. Interestingly, this effect mirrors previously reported shifts in E_{GABA} following the application of KCC2 inhibitor furosemide and acute stress [65], pointing to a possibility that PGE2 impairs KCC2 function.

Whole-Cell patch clamp replicates the PGE2 induced depolarizing shift in E_{GABA}

The whole-cell patch clamp configuration disrupts the cell's intracellular chloride composition [108,113,114]. This is due to the diffusion of the patch pipette solution in the cytoplasm [108,113,114]. Thus, depending on the intracellular solution composition and the cell being patched, the ion concentration inside the neuron may drift to non-physiological levels [113,114]. Indeed, Hewitt et al. 2009 reported that whole-cell patch-clamp induced a depolarizing shift in E_{GABA} in PVN-CRH compared to basal perforated patch recordings [65]. However, Hewitt et al. 2009 also noted that whole-cell patch-clamp was still effective in detecting a depolarizing shift in E_{GABA} induced by a KCC2 inhibitor furosemide. Furthermore, Wang et al. 2015 noted that shifts in E_{GABA} were comparable between whole-cell and perforated patch recording (in the hippocampus) [115]. Finally, Lanz et al. 2020, showed that relative changes in Cl^- homeostasis could still be tracked in whole-cell patch-clamp recordings from PVN-CRH, despite a shift in the absolute E_{GABA} values due to the replacement of intracellular Cl^- [68].

In line with these previous studies [65,68], we observed an E_{GABA} of -57.42 ± 4.57 mV under basal conditions. In addition, following PGE2 application, we saw a depolarizing shift of E_{GABA} to -49.47 ± 5.71 mV. This shift followed a similar time course to that seen in the perforated patch conditions, becoming significant by 20 minutes, but did not wash out by 40 minutes. The shift is smaller than that observed in the perforated patch experiments (whole-cell -7.55 ± 1.28 mV vs perforated patch -24.92 ± 5.31 mV). Further analysis of the current-voltage relationship showed a similar shift in intercept but not in slope.

Interestingly, the shift is similar to that reportedly induced after *in vivo* stressors [47,65]. In sum, the evidence indicates that in whole-cell patch-clamp, the effect of PGE2 on E_{GABA} could be observed.

The reasons for the smaller long-lasting shift in E_{GABA} in the whole-cell configurations compared to the perforated patch configurations are unclear. It could be that the diffusion of patch solution into the cell 'clamps' the intracellular Cl^- level to that of the patch pipette. Thus, we are unable to see rapid, strong shifts in E_{GABA} as the somatic level of $[Cl^-]_i$ will rapidly return to that of the pipette [68]. Alternatively, since the E_{GABA}'s in both conditions seem to max out around the same membrane potential, we are viewing a 'ceiling' effect of $[Cl^-]_i$ buildup [50].

PGE2-EP1 signaling mediates the depolarizing shift in E_{GABA}

A previous study that used EP1 knock-out mice demonstrated the necessity of EP1 in mediating the immune-induced activation of the HPA axis [91]. Furthermore, EP1 has been localized in the soma of PVN neurons [91,98]. Despite this evidence, the mechanism of PGE2-EP1 signaling in the PVN neurons remained unknown.

Here, we demonstrated that application of the EP1 agonist iloprost (1 μM) induced a depolarizing shift in E_{GABA}. In our experiments, the iloprost application mimicked the effects of PGE2 application – a slow depolarizing shift in E_{GABA}. In addition, similar to PGE2, there was no significant difference in the slope of the I-V curve but a significant shift in slope. This indicates EP1 induces non-synaptic changes in GABAergic signaling. Furthermore, the application of PGE2 in the presence of a competitive EP1 antagonist (GW 848687X; 1 μM) prevented PGE2-induced E_{GABA} shift. However, this prevention was only partial, as we still observed a small yet significant shift of E_{GABA} in the PGE2 + EP1 antagonist condition compared to the no-drug baseline. This is likely due to incomplete antagonism by the antagonist at the combination of drug concentrations used in the experiments.

Potential Mechanism of EP1 based depolarizing shift in E_{GABA}

Our observation that PGE2-EP1 induces changes in E_{GABA} is in line with previous work. In the spinal cord, PGE2 has been directly linked to changes in E_{GABA}, with relevance to the mechanisms underlying inflammatory pain [116]. Furthermore, molecular pathways downstream of EP1 are linked to modulation in E_{GABA}. Specifically, EP1 is a G_q-linked GPCR [89,90]. G_q exerts its downstream effects via parallel pathways: (1) release of intracellular calcium stores and (2) activation of PKC [117,118]. These pathways have distinct bidirectional effects on E_{GABA} [118]. In the hippocampus, intracellular calcium signaling has been linked to dephosphorylation of KCC2, and subsequently, a depolarizing shift in E_{GABA} [58,119]. Conversely, PKC signaling in the same neurons leads to phosphorylation and enhancement of KCC2 function, leading to a hyperpolarizing shift in E_{GABA} [120,121]. Direct experiments demonstrated that PKC and Ca^{2+} signaling pathways work concurrently to counteract their respective counterpart's effects [118]. Furthermore, in the PVN, activation of the α1 adrenergic receptor (AR)-induced a depolarizing shift in E_{GABA} similar to that observed here [65]. α1-AR is, same as EP1, a G_q-coupled GPCR that results in the release of intracellular Ca^{2+} and concurrent activation of PKC [65,101]. This

evidence guides the future directions of our study - to tease out specific downstream mechanisms for the PGE2-EP1-mediated E_{GABA} shift.

Implications in the broader scope of PGE2 signaling in the PVN

As detailed in the introduction, EP3 and EP1 have been implicated in immune-induced activation of the HPA axis [91]. Earlier studies showed that PGE2 and EP3 agonists *in vivo* and in *ex vivo* brain slices downregulate GABAergic signaling onto PVN-CRH neurons [86,95,96]. Leading to disinhibition of the HPA axis [86]. Recent work from our lab elucidated the exact synaptic mechanism of EP3 action [99]. We demonstrated that EP3 agonist application (L - 798,106) triggers suppression of GABA release onto PVN-CRH neurons from the presynaptic terminals [99]. Furthermore, this effect onset rapidly and lasted up to 15 minutes [99]. In comparison, this work demonstrated that EP1's effects show a relatively slow onset (~15-20 minutes) and can last up to 40 minutes post washout (see results). EP1 thereby may represent a method for long-term activation of the HPA axis during periods of high inflammation. In this theoretical model, EP3's effects set in rapidly following the detection of acute inflammation in the PVN; over time, the presynaptic effects of EP3 fade. In periods of sustained inflammation, EP1 signaling kicks in and weakens GABAergic input overall to PVN-CRH neurons on a longer time scale. Supporting this, EP3's effects operate on a 'per-synapse' basis, meaning some GABAergic signaling may still be operating at basal levels [104]. In contrast, EP1's effects are post-synaptic and cell-wide, meaning regardless of other GABAergic synaptic changes, GABA integration will be altered neuron-wide [50]. Further supporting this, the binding affinity of PGE2 for EP1 is much weaker than the binding affinity for EP3 [90,122]. Indicating, that EP3 shows increased sensitivity to weaker inflammation than EP1 [94].

Limitations

As noted previously, whole-cell patch-clamp can introduce errors into the measurements of ionic equilibrium [68,108,113,114]. This is due to the diffusion of the internal patch-clamp solution into the cytosol of the cell [108,113,114]. This results in artificial changes in ionic concentration and subsequently shifts in the equilibrium potential (see methods) [108,114]. Furthermore, long recording times – such as those used in this experiment – may facilitate complete diffusion between the two compartments [114], and thus skew the measurement of E_{GABA}. In our experiments, we addressed this potential limitation as follows: First, we validated

the role of PGE2 signaling using the gramicidin perforated patch technique. Gramicidin creates small ionophores within the cell membrane that allow ions (namely Na^+ and K^+) to pass thru, but crucially, not Cl^- [108]. This allows the command of the membrane potential without disrupting intracellular Cl^- concentration [108]. Using this, we validated the effects of PGE2 on Cl^-. In addition, for our whole-cell experiments, we performed both within-cell and between-cell recordings for our drug wash-on (see methods). In 'within-cell' experiments, the same cell was held prior-to and following drug wash-on for up to 60 minutes. To account for the errors introduced by long recording times, we also introduced 'between-cell' experiments. In 'between-cell' experiments, cells recordings were initiated (i.e., whole-cell configuration was obtained) in separate cells before and after drug application. Cells were only held for a short time period to complete the E_{GABA} measurement (~5 minutes).

In our experiments, we used EtOH (final concentration 0.01%; ~1 μM) as a vehicle to dissolve PGE2, EP1 agonist, and EP1 antagonist. This has the potential to introduce error because EtOH is a potent modulator of GABAergic signaling in the CNS [123]. The precise effects are brain region-dependent [123,124]. For example, in the amygdala, EtOH administration (44mM) potentiated GABAergic signaling [125]. To control for this, we introduced a vehicle control (EtOH; 0.01%; ~1 μM) in both perforated- and whole-cell patch-clamp experiments. Notably, wash-on of ethanol alone seemed to induce no significant effect on E_{GABA} when measured via the muscimol puff method (for both perforated and whole-cell experiments). Indicating that the EtOH vehicle at the concentration used in this experiment did not cause detectable changes in E_{GABA}.

This experiment specifically measured the effect of PGE2 on changes in somatic $[Cl^-]_i$ homeostasis. The theoretical discussions above and below operate under the assumption of an isopotential neuron, and therefore somatic $[Cl^-]_i$ homeostasis influences GABA signaling cell-wide. In reality, the interaction between dendritic-, somatic-, axonal- compartmentalization, and localization of $[Cl^-]_i$ homeostatic mediators (KCC2, NKCC1) creates a complex gradient of Cl^- across the neuron [104]. In turn, E_{GABA} can be temporally and directionally different depending on the synapse localization [104]. Recent work by Lanz et al. 2020 suggests a distinct temporal difference between $[Cl^-]_i$ extrusion in the dendrites and soma of PVN-CRH neurons [68]. More specifically, following acute stress, the Cl^-gradient collapsed rapidly in synaptic compartments

during periods of high-frequency synaptic stimulation, leading to excitatory GABAergic signaling [68]. In comparison, the somatic Cl^-gradient was shown to be much more robust to high-frequency stimulation and did not collapse into excitatory GABAergic signaling following acute stress [68]. Further experiments will be needed in order to understand how PGE2 – E_{GABA} relationships are shaped spatially within the cell.

Future Directions

As noted above, one important future study is to tease out the intracellular molecular pathways which mediate the PGE2-EP1 effect on PGE2. Our prediction is that EP1, through G_q, triggers downregulation of KCC2 function (see Potential Mechanism of EP1 based depolarizing shift in E_{GABA}). In turn, the cell cannot regulate Cl^- homeostasis, and we see a depolarizing shift in E_{GABA}. Based on this theory, we can generate two potential hypotheses for further testing: (1) the intracellular application of a calcium chelator (e.g. BAPTA) should block this signaling pathway and prevent the modulation of E_{GABA} (as demonstrated in [57,58]). (2) Considering that PKC counteracts the effects of Ca^{2+} signaling, the intracellular application of a PKC inhibitor (e.g. calphostin) should enhance the depolarizing shift (as demonstrated in [118]). (3) an application of KCC2 inhibitor furosemide should mimic and occlude the effect of PGE2 signaling on E_{GABA} (as demonstrated in [47,65])

The stress response shows sexual dimorphism in its magnitude and temporal characteristics [126–128]. Reflecting this, the PVN-CRH neurons show sexual dimorphism in their electrophysiological [129] and molecular [126,128,130] characteristics. Similarly, the immune system functions in a sexually dimorphic manner [126,131]. Moreover, the interaction between the immune system and the HPA axis shows sex differences [126,128,132]. Endogenous PGE2 release via astrocytes in the hypothalamus triggers activation of gonadotropin-releasing hormone (GnRH) neurons, a pathway necessary in female maturation and ovulation [133,134]. Combined, the evidence points towards a potential sexual dimorphism in the pathways explored here. The present study was completed only on male mice. Future experiments should include a female cohort. Given the above evidence, we anticipate a potential sexually dimorphic response to the application of PGE2 on PVN-CRH neurons.

Significance & Conclusion

The interaction between the HPA axis and the immune system is critical in the regulation of immune and stress responses in the body [117,135]. GCs functions as a critical negative feedback signal onto the immune system [12]. Previously studies showed that PGE2 via EP1 and EP3 mediates the immune-induced activation of the HPA axis [86] [91].

Our project revealed the ability of PGE2-EP1 signaling to cause a depolarizing shift in E_{GABA}, which will result in disinhibition (excitation) of PVN-CRH neurons. These results are congruent with other results showing shifts in E_{GABA} as a form of metaplasticity in the PVN [14]. In addition, we theorized the potential implications of these results in conjunction with other PGE2 signaling pathways in the PVN. We theorized that the longer time scale of PGE2-EP1 signaling observed here complements the shorter time scale of PGE2-EP3 signaling we previously reported [136]. This may represent the ability of the PVN to respond biphasically to inflammation.

In the broader scope, the results here could have potential clinical implications. Dysregulated immune to HPA communication has been implicated in many conditions [137], including sepsis [138], HIV [139], and depression [132]. PGE2 synthesis inhibitors (such as COX inhibitors) have been investigated as a therapeutic for psychiatric disorders [140]. A better understanding of the mechanistic pathways by which inflammation activates the HPA axis – such as the result achieved here – creates the potential for more specific therapeutic interventions down the line.

References

1 Taborsky, B. *et al.* (2021) Towards an Evolutionary Theory of Stress Responses. *Trends Ecol. Evol.* 36, 39–48

2 Boyce, W.T. and Ellis, B.J. (2005) Biological sensitivity to context: I. An evolutionary-developmental theory of the origins and functions of stress reactivity. *Dev. Psychopathol.* 17, 271–301

3 Ulrich-Lai, Y.M. and Herman, J.P. (2009) Neural regulation of endocrine and autonomic stress responses. *Nat. Rev. Neurosci.* 10, 397–409

4 McCarty, R. (2016) *The Fight-or-Flight Response: A Cornerstone of Stress Research*, Elsevier Inc.

5 Biag, J. *et al.* (2012) Cyto- and chemoarchitecture of the hypothalamic paraventricular nucleus in the C57BL/6J male mouse: A study of immunostaining and multiple fluorescent tract tracing. *J. Comp. Neurol.* 520, 6–33

6 Palkovits, M. (1984) Neuropeptides in the hypothalamo-hypophyseal system: Lateral retrochiasmatic area as a common gate for neuronal fibers towards the median eminence. *Peptides* 5, 35–39

7 Romanov, R.A. *et al.* (2015) A secretagogin locus of the mammalian hypothalamus controls stress hormone release. *EMBO J.* 34, 36–54

8 Makara, G.B. *et al.* (1981) Effects of paraventricular lesions on stimulated ACTH release and CRF in stalk-median eminence of the rat. *Am. J. Physiol. - Endocrinol. Metab.* 3, 441–446

9 Aguilera, G. and Liu, Y. (2012) The molecular physiology of CRH neurons. *Front. Neuroendocrinol.* 33, 67–84

10 Bellavance, M.A. and Rivest, S. The HPA - immune axis and the immunomodulatory actions of glucocorticoids in the brain. , *Frontiers in Immunology*, 5. (2014) , Frontiers Media S.A.

11 Baschant, U. and Tuckermann, J. (2010) The role of the glucocorticoid receptor in

inflammation and immunity. *J. Steroid Biochem. Mol. Biol.* 120, 69–75

12 Timmermans, S. *et al.* (2019) A general introduction to glucocorticoid biology. *Front. Immunol.* 10,

13 Levy, B.H. and Tasker, J.G. (2012) Synaptic regulation of the hypothalamic–pituitary–adrenal axis and its modulation by glucocorticoids and stress. *Front. Cell. Neurosci.* 6, 1–13

14 Fujioka, T. *et al.* (2001) Mild prenatal stress enhances learning performance in the non-adopted rat offspring. *Neuroscience* 103,

15 Feetham, C.H. *et al.* (2018) Ion channels in the paraventricular hypothalamic nucleus (PVN); Emerging diversity and functional roles. *Front. Physiol.* 9, 1–23

16 Van Den Pol, A.N. (1982) The magnocellular and parvocellular paraventricular nucleus of rat: Intrinsic organization. *J. Comp. Neurol.* 206, 317–345

17 Sawchenko, P.E. *et al.* (1984) Co-expression of corticotropin-releasing factor and vasopressin immunoreactivity in parvocellular neurosecretory neurons of the adrenalectomized rat (co-localization/hypothalamus/immunohistochemistry/neurohypophysial peptide/paraventricular nucleus). *Neurobiology* 81, 1883–1887

18 Wamsteeker Cusulin, J.I. *et al.* (2013) Characterization of Corticotropin-Releasing Hormone neurons in the Paraventricular Nucleus of the Hypothalamus of Crh-IRES-Cre Mutant Mice. *PLoS One* 8, 1–10

19 Brown, C.H. *et al.* (2013) *Physiological regulation of magnocellular neurosecretory cell activity: Integration of intrinsic, local and afferent mechanisms*, 25

20 Prager-Khoutorsky, M. and Bourque, C.W. (2015) Mechanical Basis of Osmosensory Transduction in Magnocellular Neurosecretory Neurones of the Rat Supraoptic Nucleus. *J. Neuroendocrinol.* 27, 507–515

21 Sudbury, J.R. *et al.* (2010) Osmotic and thermal control of magnocellular neurosecretory neurons - role of an N-terminal variant of trpv1. *Eur. J. Neurosci.* 32, 2022–2030

22 Antunes-rodrigues, J. *et al.* (2006) Neuroendocrine Control of Body Fluid Metabolism Neuroendocrine Control of Body Fluid Metabolism. *Control* DOI: 10.1152/physrev.00017.2003

23 Badaut, J. *et al.* (2000) Hypervascularization in the magnocellular nuclei of the rat hypothalamus: Relationship with the distribution of aquaporin-4 and markers of energy metabolism. *J. Neuroendocrinol.* 12, 960–969

24 Feetham, C.H. *et al.* (2015) TRPV4 and KCa ion channels functionally couple as osmosensors in the paraventricular nucleus. *Br. J. Pharmacol.* 172, 1753–1768

25 Stern, J.E. (2001) Electrophysiological and morphological properties of pre-autonomic neurones in the rat hypothalamic paraventricular nucleus. *J. Physiol.* 537, 161–177

26 Makino, S. *et al.* (2005) Expression of type 1 corticotropin-releasing hormone (CRH) receptor mRNA in the hypothalamic paraventricular nucleus following restraint stress in CRH-deficient mice. *Brain Res.* 1048, 131–137

27 Elliott, E. *et al.* (2010) Resilience to social stress coincides with functional DNA methylation of the Crf gene in adult mice. *Nat. Neurosci.* 13, 1351–1353

28 Ramot, A. *et al.* (2017) Hypothalamic CRFR1 is essential for HPA axis regulation following chronic stress. *Nat. Neurosci.* 20, 385–388

29 Swanson, L.W. and Sawchenko, P.E. (1983) Hypothalamic integration: Organization of the paraventricular and supraoptic nuclei. *Annu. Rev. Neurosci.* Vol. 6, 269–324

30 Ritter, S. *et al.* (2003) Immunotoxin lesion of hypothalamically projecting norepinephrine and epinephrine neurons differentially affects circadian and stressor-stimulated corticosterone secretion. *Endocrinology* 144, 1357–1367

31 Herman, J.P. *et al.* (2003) Central mechanisms of stress integration: Hierarchical circuitry controlling hypothalamo-pituitary-adrenocortical responsiveness. *Front. Neuroendocrinol.* 24, 151–180

32 Herman, J.P. *et al.* (2005) Limbic system mechanisms of stress regulation: Hypothalamo-pituitary- adrenocortical axis. *Prog. Neuro-Psychopharmacology Biol. Psychiatry* 29,

1201–1213

33 Herman, J.P. *et al.* (1995) Contribution of the Ventral Subiculum to Inhibitory Regulation of the Hypothalamo-Pituitary-Adrenocortical Axis. *J. Neuroendocrinol.* 7, 475–482

34 Herman, J.P. *et al.* (2020) Brain mechanisms of HPA axis regulation: neurocircuitry and feedback in context Richard Kvetnansky lecture. *Stress* 23, 617–632

35 Sullivan, G.M. *et al.* (2004) Lesions in the bed nucleus of the stria terminalis disrupt corticosterone and freezing responses elicited by a contextual but not by a specific cue-conditioned fear stimulus. *Neuroscience* 128, 7–14

36 Miklós, I.H. and Kovács, K.J. (2002) GABAergic innervation of corticotropin-releasing hormone (CRH)-secreting parvocellular neurons and its plasticity as demonstrated by quantitative immunoelectron microscopy. *Neuroscience* 113, 581–592

37 Miklos, I.H. *et al.* (2012) Reorganization of synaptic inputs to the hypothalamic paraventricular nucleus during chronic psychogenic stress in rats. *Biol. Psychiatry* 71, 301–308

38 Cole, R.L. and Sawchenko, P.E. (2002) Neurotransmitter regulation of cellular activation and neuropeptide gene expression in the paraventricular nucleus of the hypothalamus. *J. Neurosci.* 22, 959–969

39 Cullinan, W.E. *et al.* (2008) Functional role of local GABAergic influences on the HPA axis. *Brain Struct. Funct.* 213, 63–72

40 Han, S.K. *et al.* (2002) Noradrenaline excites and inhibits GABAergic transmission in parvocellular neurons of rat hypothalamic paraventricular nucleus. *J. Neurophysiol.* 87, 2287–2296

41 Inoue, W. and Bains, J.S. (2014) Beyond inhibition: GABA synapses tune the neuroendocrine stress axis. *BioEssays* 36, 561–569

42 Hill, M.N. and Tasker, J.G. (2012) Endocannabinoid signaling, glucocorticoid-mediated negative feedback, and regulation of the hypothalamic-pituitary-adrenal axis. *Neuroscience* 204, 5–16

43 Hill, M.N. *et al.* (2011) Recruitment of prefrontal cortical endocannabinoid signaling by glucocorticoids contributes to termination of the stress response. *J. Neurosci.* 31, 10506–10515

44 Jiang, Z. *et al.* (2019) CRF signaling between neurons in the paraventricular nucleus of the hypothalamus (PVN) coordinates stress responses. *Neurobiol. Stress* 11, 100192

45 Jiang, Z. *et al.* (2018) Local Corticotropin-Releasing Factor Signaling in the Hypothalamic Paraventricular Nucleus. *J. Neurosci.* 38, 1874–1890

46 Inoue, W. *et al.* (2013) Noradrenaline is a stress-associated metaplastic signal at GABA synapses. *Nat. Neurosci.* 16, 605–612

47 Gao, Y. and Zhou, J.-J. (2017) Chronic unpredictable mild stress induces loss of GABA inhibition in corticotrophin-releasing hormone-expressing neurons through NKCC1 upregulation. *Neuroendocrinology* 33, 395–401

48 Verkuyl, J.M. *et al.* (2004) Chronic stress attenuates GABAergic inhibition and alters gene expression of parvocellular neurons in rat hypothalamus. *Eur. J. Neurosci.* 20, 1665–1673

49 Staley, K.J. and Proctor, W.R. (1999) Modulation of mammalian dendritic GABA(A) receptor function by the kinetics of Cl- and HCO3- transport. *J. Physiol.* 519, 693–712

50 Doyon, N. *et al.* (2016) Chloride Regulation: A Dynamic Equilibrium Crucial for Synaptic Inhibition. *Neuron* 89, 1157–1172

51 Ganguly, K. *et al.* (2001) GABA itself promotes the developmental switch of neuronal GABAergic responses from excitation to inhibition. *Cell* 105, 521–532

52 Blaesse, P. *et al.* (2006) Oligomerization of KCC2 correlates with development of inhibitory neurotransmission. *J. Neurosci.* 26, 10407–10419

53 Doyon, N. *et al.* (2016) Mild KCC2 hypofunction causesinconspicuous chloride dysregulation that degrades neural coding. *Front. Cell. Neurosci.* 9,

54 Authement, M.E. *et al.* (2015) Histone Deacetylase Inhibition Rescues Maternal Deprivation-Induced GABAergic Metaplasticity through Restoration of AKAP Signaling.

Neuron 86, 1240–1252

55 Pisella, L.I. *et al.* (2019) Impaired regulation of KCC2 phosphorylation leads to neuronal network dysfunction and neurodevelopmental pathology. *Sci. Signal.* 12,

56 Perkins, K.L. and Wong, R.K.S. (1996) Ionic basis of the postsynaptic depolarizing GABA response in hippocampal pyramidal cells. *J. Neurophysiol.* 76, 3886–3894

57 Woodin, M.A. *et al.* (2003) Coincident Pre-and Postsynaptic Activity Modifies GABAergic Synapses by Postsynaptic Changes in Cl Transporter Activity At many excitatory synapses, coincident pre-and postsynaptic spiking of different temporal patterns has been shown to result in either . *Neuron* 39, 807–820

58 Fiumelli, H. *et al.* (2005) Modulation of GABAergic transmission by activity via postsynaptic Ca 2+-dependent regulation of KCC2 function. *Neuron* 48, 773–786

59 Ferrini, F. *et al.* (2020) Differential chloride homeostasis in the spinal dorsal horn locally shapes synaptic metaplasticity and modality-specific sensitization. *Nat. Commun.* 11,

60 Taylor, A.M.W. *et al.* (2016) Neuroimmune Regulation of GABAergic Neurons Within the Ventral Tegmental Area during Withdrawal from Chronic Morphine. *Neuropsychopharmacology* 41, 949–959

61 Ostroumov, A. *et al.* (2016) Stress Increases Ethanol Self-Administration via a Shift toward Excitatory GABA Signaling in the Ventral Tegmental Area. *Neuron* 92, 493–504

62 Ye, Z.-Y. *et al.* (2012) NKCC1 Upregulation Disrupts Chloride Homeostasis in the Hypothalamus and Increases Neuronal Activity-Sympathetic Drive in Hypertension. *J. Neurosci.* 32, 8560–8568

63 Kim, Y.B. *et al.* (2018) Excitatory GABAergic action and increased vasopressin synthesis in hypothalamic magnocellular neurosecretory cells underlie the high plasma level of vasopressin in diabetic rats. *Diabetes* 67, 486–495

64 Kim, Y.B. *et al.* Long-term ionic plasticity of GABAergic signalling in the hypothalamus. , *Journal of Neuroendocrinology*. (2019) , Blackwell Publishing Ltd

65 Hewitt, S.A. *et al.* (2009) Altered chloride homeostasis removes synaptic inhibitory

constraint of the stress axis. *Nat. Neurosci.* 12, 438–443

66 Sarkar, J. *et al.* (2011) Neurosteroidogenesis Is Required for the Physiological Response to Stress: Role of Neurosteroid-Sensitive GABAA Receptors. *J. Neurosci.* 31, 18198–18210

67 Lanz, A.J. (2019) , Chloride Dynamics and the Control of CRH Activity. , UNIVERSITY OF CALGARY Chloride

68 Lanz, A. *et al.* (2020) Spatiotemporal chloride dynamics in hypothalamic CRH PVN neurons. DOI: 10.1101/2020.05.29.122432

69 Bergeron, M.J. *et al.* (2006) Identification of key functional domains in the C terminus of the K +-Cl- cotransporters. *J. Biol. Chem.* 281, 15959–15969

70 Kotas, M.E. and Mezhitov, R. (2015) Homeostasis, Inflammation, and Disease Susceptibility. *Cell* 160, 816–827

71 Abbas, A.K. *et al.* (2015) Innate Immunity: The Early Defense Against Infections. In *Basic Immunology: Functions and Disorders of the Immune System* Fifth. (Abbas, A. K. et al., eds), pp. 24, Elsevier

72 Varatharaj, A. and Galea, I. The blood-brain barrier in systemic inflammation. , *Brain, Behavior, and Immunity*, 60. 01-Feb-(2017) , Academic Press Inc., 1–12

73 Holzer, P. *et al.* Visceral inflammation and immune activation stress the brain. , *Frontiers in Immunology*, 8. 22-Nov-(2017) , Frontiers Media S.A.

74 Firmino, M. *et al.* (2018) Label-free quantitative proteomics of rat hypothalamus under fever induced by LPS and PGE2. *J. Proteomics* 187, 182–199

75 Lazarus, M. (2006) The differential role of prostaglandin E2 receptors EP3 and EP4 in regulation of fever. *Mol. Nutr. Food Res.* 50, 451–455

76 Kakizaki, Y. *et al.* (1999) Temporal Profiles of Interleukin-1.BETA., Interleukin-6, and Tumor Necrosis Factor-.ALPHA. in the Plasma and Hypothalamic Paraventricular Nucleus after Intravenous or Intraperitoneal Administration of Lipopolysaccharide in the Rat. Estimation by Push-Pull. *Endocr. J.* 46, 487–496

77 Wan, W. *et al.* (1993) Differential induction of c-Fos immunoreactivity in hypothalamus and brain stem nuclei following central and peripheral administration of endotoxin. *Brain Res. Bull.* 32, 581–587

78 Elenkov, I.J. *et al.* (1992) Lipopolysaccharide is able to bypass corticotrophin-releasing factor in affecting plasma ACTH and corticosterone levels: Evidence from rats with lesions of the paraventricular nucleus. *J. Endocrinol.* 133, 231–236

79 Dantzer, R. (2018) Neuroimmune interactions: From the brain to the immune system and vice versa. *Physiol. Rev.* 98, 477–504

80 Butler, L.D. *et al.* (1989) Neuroendocrine regulation of in vivo cytokine production and effects: I. In vivo regulatory networks involving the neuroendocrine system, interleukin-1 and tumor necrosis factor-α. *J. Neuroimmunol.* 24, 143–153

81 Bertini, R. *et al.* (1988) Adrenalectomy sensitizes mice to the lethal effects of interleukin 1 and tumor necrosis factor. *J. Exp. Med.* 167, 1708–1712

82 Ruzek, M.C. *et al.* (1999) Endogenous glucocorticoids protect against cytokine-mediated lethality during viral infection. *J. Immunol.* 162, 3527–33

83 Busillo, J.M. and Cidlowski, J.A. The five Rs of glucocorticoid action during inflammation: Ready, reinforce, repress, resolve, and restore. , *Trends in Endocrinology and Metabolism*. (2013)

84 Brouckaert, P. *et al.* (1992) The glucocorticoid antagonist RU38486 mimics interleukin-1 in its sensitization to the lethal and interleukin-6-inducing properties of tumor necrosis factor. *Eur. J. Immunol.* 22, 981–986

85 Garcia-Bueno, B. *et al.* (2009) Cerebrovascular Cyclooxygenase-1 Expression, Regulation, and Role in Hypothalamic-Pituitary-Adrenal Axis Activation by Inflammatory Stimuli. *J. Neurosci.* 29, 12970–12981

86 Ferri, C.C. and Ferguson, A. V. (2005) Prostaglandin E2 mediates cellular effects of interleukin-1β on parvocellular neurones in the paraventricular nucleus of the hypothalamus. *J. Neuroendocrinol.* 17, 498–508

87 Quan, N. *et al.* (2003) Endothelial activation is an intermediate step for peripheral lipopolysaccharide induced activation of paraventricular nucleus. *Brain Res. Bull.* 59, 447–452

88 Ricciotti, E. and Fitzgerald, G.A. (2011) Prostaglandins and inflammation. *Arterioscler. Thromb. Vasc. Biol.* 31, 986–1000

89 Furuyashiki, T. and Narumiya, S. (2011) Stress responses: The contribution of prostaglandin E2 and its receptors. *Nat. Rev. Endocrinol.* 7, 163–175

90 Narumiya, S. *et al.* (1999) Prostanoid Receptors: Structures, Properties, and Functions. *Physiol. Rev.* 79, 1193–1226

91 Matsuoka, Y. *et al.* (2003) Impaired adrenocorticotropic hormone response to bacterial endotoxin in mice deficient in prostaglandin E receptor EP1 and EP3 subtypes. *Proc. Natl. Acad. Sci.* 100, 4132–4137

92 Serrats, J. *et al.* (2017) Pro-inflammatory immune-to-brain signaling is involved in neuroendocrine responses to acute emotional stress. *Brain. Behav. Immun.* 62, 53–63

93 Furuyashiki, T. and Narumiya, S. (2009) Roles of prostaglandin E receptors in stress responses. *Curr. Opin. Pharmacol.* 9, 31–38

94 Markovič, T. *et al.* (2017) Structural features of subtype-selective EP receptor modulators. *Drug Discov. Today* 22, 57–71

95 Zhang, Z.-H. *et al.* (2011) EP 3 receptors mediate PGE 2 -induced hypothalamic paraventricular nucleus excitation and sympathetic activation. *Am. J. Physiol. Circ. Physiol.* 301, H1559–H1569

96 Yamaguchi, N. *et al.* (2019) Prostaglandin E2 receptor EP3 subtype in the paraventricular hypothalamic nucleus mediates corticotropin-releasing factor-induced elevation of plasma noradrenaline levels in rats. *Eur. J. Pharmacol.* 863, 172693

97 Oka, T. *et al.* (2000) Relationship of EP1-4 prostaglandin receptors with rat hypothalamic cell groups involved in lipopolysaccharide fever responses. *J. Comp. Neurol.* 428, 20–32

98 Lv, L. *et al.* (2021) The PGE2 receptor EP3 plays a positive role in the activation of

hypothalamic-pituitary-adrenal axis and neuronal activity in the hypothalamus under immobilization stress. *Brain Res. Bull.* 168, 45–51

99 Khazaeipool, Z. *et al.* (2018) Prostaglandin E2 depresses GABA release onto parvocellular neuroendocrine neurones in the paraventricular nucleus of the hypothalamus via presynaptic receptors. *J. Neuroendocrinol.* 30, 1–10

100 Zhang, J. and Rivest, S. (1999) Distribution, regulation and colocalization of the genes encoding the EP2- and EP4-PGE2 receptors in the rat brain and neuronal responses to systemic inflammation. *Eur. J. Neurosci.* 11, 2651–2668

101 Perez, D.M. (2020) α1-Adrenergic Receptors in Neurotransmission, Synaptic Plasticity, and Cognition. *Front. Pharmacol.* 11, 1–22

102 Luther, J.A. and Tasker, J.G. (2000) Voltage-gated currents distinguish parvocellular from magnocellular neurones in the rat hypothalamic paraventricular nucleus. *J. Physiol.* 523, 193–209

103 Sakmann, B. and Neher, E. (1995) *Single-Channel Recording*, Springer Science+Business Media New York.

104 Doyon, N. *et al.* (2011) Efficacy of synaptic inhibition depends on multiple, dynamically interacting mechanisms implicated in chloride homeostasis. *PLoS Comput. Biol.* 7,

105 Luhmann, H.J. *et al.* (2014) Comment on "Local impermeant anions establish the neuronal chloride concentration." *Science (80-.).* 345, 1130c

106 Taglialatela, M. *et al.* (1992) Novel voltage clamp to record small, fast currents from ion channels expressed in Xenopus oocytes. *Biophys. J.* 61, 78–82

107 Kyrozis, A. and Reichling, D.B. (1995) Perforated-patch recording with gramicidin avoids artifactual changes in intracellular chloride concentration. *J. Neurosci. Methods* 57, 27–35

108 Harata, N. and Akaike, N. (1995) Gramicidin-perforated patch recording: GABA response in mammalian. *Physiology*

109 DeFazio, R.A. *et al.* (2000) Potassium-coupled chloride cotransport controls intracellular chloride in rat neocortical pyramidal neurons. *J. Neurosci.* 20, 8069–8076

110 Yang, B. *et al.* (2015) Regulation of GABA equilibrium potential by mGluRs in rat hippocampal CA1 neurons. *PLoS One* 10, 1–16

111 Suri, D. *et al.* (2013) Early stress evokes age-dependent biphasic changes in hippocampal neurogenesis, Bdnf expression, and cognition. *Biol. Psychiatry* 73, 658–666

112 Liu, J. and Wang, Y.T. (2014) Allosteric modulation of GABAA receptors by extracellular ATP. *Mol. Brain* 7, 1–11

113 Oliva, C. *et al.* (1988) Calculation of time constants for intracellular diffusion in whole cell patch clamp configuration. *Biophys. J.* 54, 791–799

114 Mathias, R.T. *et al.* (1990) Limitations of the whole cell patch clamp technique in the control of intracellular concentrations. *Biophys. J.* 58, 759–770

115 Wang, B. *et al.* (2015) A subtype of inhibitory interneuron with intrinsic persistent activity in human and monkey neocortex. *Cell Rep.* 10, 1450–1458

116 Funk, K. *et al.* (2008) Modulation of chloride homeostasis by inflammatory mediators in dorsal root ganglion neurons. *Mol. Pain* 4, 1–12

117 Furuyashiki, T. and Narumiya, S. (2011) Stress responses: The contribution of prostaglandin E2and its receptors. *Nat. Rev. Endocrinol.* 7, 163–175

118 Lee, H.H.C. *et al.* (2011) NMDA receptor activity downregulates KCC2 resulting in depolarizing GABAA receptor-mediated currents. *Nat. Neurosci.* 14, 736–743

119 Lee, H.H.C. *et al.* (2007) Direct protein kinase C-dependent phosphorylation regulates the cell surface stability and activity of the potassium chloride cotransporter KCC2. *J. Biol. Chem.* 282, 29777–29784

120 Kfir, A. *et al.* (2020) A Cellular Mechanism of Learning-Induced Enhancement of Synaptic Inhibition: PKC-Dependent Upregulation of KCC2 Activation. *Sci. Rep.* 10, 1–11

121 Kahle, K.T. *et al.* (2013) Modulation of neuronal activity by phosphorylation of the K-Cl cotransporter KCC2. *Trends Neurosci.* 36, 726–737

122 Jones, R.L. *et al.* (2009) Prostanoid receptor antagonists: Development strategies and

therapeutic applications. *Br. J. Pharmacol.* 158, 104–145

123 Davies, M. (2003) The role of GABAA receptors in mediating the effects of alcohol in the central nervous system. *J. Psychiatry Neurosci.* 28, 263–274

124 Jia, F. *et al.* (2008) Ethanol modulates synaptic and extrasynaptic GABAA receptors in the thalamus. *J. Pharmacol. Exp. Ther.* 326, 475–482

125 Jimenez, V.A. *et al.* (2019) Synaptic adaptations in the central amygdala and hypothalamic paraventricular nucleus associated with protracted ethanol abstinence in male rhesus monkeys. *Neuropsychopharmacology* 44, 982–993

126 Vamvakopoulos, N. (1995) Sexual dimorphism of stress response and immune/ inflammatory reaction" the corticotropin releasing hormone perspective. *Rev. Pap. Mediat. Inflamm.* 4, 163–174

127 Zuena, A.R. *et al.* (2008) Prenatal restraint stress generates two distinct behavioral and neurochemical profiles in male and female rats. *PLoS One* 3,

128 Oyola, M.G. and Handa, R.J. (2017) Hypothalamic–pituitary–adrenal and hypothalamic–pituitary–gonadal axes: sex differences in regulation of stress responsivity. *Stress* 20, 476–494

129 Senst, L. (2014) , Stress, sex and synapses: an exploration of stress-associated male/female differences in electrophysiological properties of corticotropin-releasing hormone neurons of the paraventricular nucleus of the hypothalamus.

130 Sterrenburg, L. *et al.* (2011) Chronic stress induces sex-specific alterations in methylation and expression of corticotropin-releasing factor gene in the rat. *PLoS One* 6, 1–14

131 Homo-Delarche, F. *et al.* (1991) Sex steroids, glucocorticoids, stress and autoimmunity. *J. Steroid Biochem. Mol. Biol.* 40, 619–637

132 Bekhbat, M. and Neigh, G. (2017) Sex differences in the neuro-immune consequences of stress: Focus on depression and anxiety. *Brain. Behav. Immun.* 176, 139–148

133 Clasadonte, J. and Prevot, V. (2018) The special relationship: Glia-neuron interactions in the neuroendocrine hypothalamus. *Nat. Rev. Endocrinol.* 14, 25–44

134 Parent, A.S. *et al.* (2008) Oxytocin facilitates female sexual maturation through a glia-to-neuron signaling pathway. *Endocrinology* 149, 1358–1365

135 Gadek-Michalska, A. *et al.* (2013) Cytokines, prostaglandins and nitric oxide in the regulation of stress-response systems. *Pharmacol. Reports* 65, 1655–1662

136 Wiederman, M. (2019) , Psychological stress modulates synaptic mechanisms for prostaglandin E2-mediated HPA axis activation. , University of Western Ontario

137 Michopoulos, V. *et al.* (2017) Inflammation in Fear-and Anxiety-Based Disorders: PTSD, GAD, and beyond. *Neuropsychopharmacology* 42, 254–270

138 Schroeder, S. *et al.* (2001) The hypothalamic-pituitary-adrenal axis of patients with severe sepsis: Altered response to corticotropin-releasing hormone. *Crit. Care Med.* 29, 310–316

139 George, M.M. and Bhangoo, A. (2013) Human immune deficiency virus (HIV) infection and the hypothalamic pituitary adrenal axis. *Rev. Endocr. Metab. Disord.* 14, 105–112

140 Sethi, R. *et al.* (2019) Neurobiology and Therapeutic Potential of Cyclooxygenase-2 (COX-2) Inhibitors for Inflammation in Neuropsychiatric Disorders. *Front. Psychiatry* 10, 1–21

CV: SAM MESTERN

Education

University of Western Ontario
M.Sc. Neuroscience **2019-2021**
Research Area: "The role of inflammation in stress signaling & hypothalamic plasticity."

Carleton University
Bachelor of Science Honours Neuroscience and Mental Health **2014 - 2019**
With High Distinction
Minor: Psychology
Honours thesis: "Effects of various early life psychological stressors on plasticity in the rat hippocampus."

Awards

CONP Scholars Award - 15,000 **2020 - 2021**
Deans' Honour List **2015 – 2016**
George Fierheller Scholarship **2016**

Research Experience

Inoue Lab – Robarts Research Institute - Western University
Research Assistant **2019 -**

- Patch-clamp electrophysiologist with specific focus on pharmacological applications
- Immunohistochemistry and other wet lab techniques.
- Computational focus on data visualization and feature extraction from electrophysiological waveforms

Forensic Research Unit – Institute of Mental Health Research – The Royal Ottawa Hospital
Volunteer Research Assistant **2018 - 2019**

- Working with patient clinical data. Including health records, and court proceedings.
- Day-to-day tasks include data entry (SPSS 25), organisation and qualitative data coding.

Presentations

Mestern, S. Benigno, G., Ichiyama, A., Inoue, W., Muller, L., (July 3, 2020) *A neuron-to-network computational model of state-dependent computation in hypothalamus.* OCNS – CNS*2021. Online.

Posters

Mestern, S., Wiederman, M., Inoue, W. (Nov 4, 2020) *Prostaglandin E2 alters intracellular chloride homeostasis to drive neuroendocrine stress response to immune challenges*. Physiology and Pharmacology Research Day, Dept. of Physiology and Pharmacology, University of Western Ontario, London, ON. – **Winner of Neuroscience Poster award**

Mestern, S., Ghazal, S., Alam, F., Beaudette, T., Zeidan, N., Johnson, W. (March 4, 2019) *First Nations Communities and the Debilitating Impact from Natural Disasters*. PHACtually Speaking Seminar, Public Health Agency of Canada, Ottawa, ON.

Healey, L., Mathias, M. & Mestern, S. (June 27, 2019) *A missing step? Outcomes of fitness and criminal responsibility assessments in referrals from communities without Mental Health Courts.* International Association of Forensic Mental Health Services 2019 Annual Conference, Montreal, Quebec.

External Projects

Mestern, S*. pyAPisolation.* (2019) – Python program to automatically extract & analyze action potentials from intracellular electrophysiological waveforms. *Open Source under MIT license*

Mestern, S. *pyCEDFS.* (2021) – Software to open and manipulate CFS files (Created by CED patch-clamp software) in python. Also allows conversion to the open science neuroscience without borders (NWB) format. *Open Source under MIT license*

Contributing Writer – Society of Neuroscience Graduate Students (SONGS) **2019 -**
The Dorsal Column

Backend developer – The JMT Primate Cell-Type Database **2019 –**
Ex Vivo Data - Electrophysiology – Built the pipeline to deliver raw experimental data in a format more accessible to the user. Built process to tabulate and visualize the data in browser.